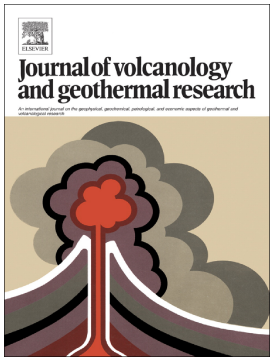

The 1994–2001 eruptive period at Rabaul, Papua New Guinea: Petrological and geochemical evidence for basalt injections into a shallow dacite magma reservoir, and significant SO2 flux

H. Patia, S.M. Eggins, R.J. Arculus, C.O. McKee, R.W. Johnson, A. Bradney

PII: S0377-0273(17)30214-7
DOI: doi: 10.1016/j.jvolgeores.2017.08.011
Reference: VOLGEO 6181

To appear in: *Journal of Volcanology and Geothermal Research*

Received date: 9 April 2017
Revised date: 26 August 2017
Accepted date: 26 August 2017

Please cite this article as: H. Patia, S.M. Eggins, R.J. Arculus, C.O. McKee, R.W. Johnson, A. Bradney , The 1994–2001 eruptive period at Rabaul, Papua New Guinea: Petrological and geochemical evidence for basalt injections into a shallow dacite magma reservoir, and significant SO2 flux, *Journal of Volcanology and Geothermal Research* (2017), doi: 10.1016/j.jvolgeores.2017.08.011

The 1994-2001 eruptive period at Rabaul, Papua New Guinea: petrological and geochemical evidence for basalt injections into a shallow dacite magma reservoir, and significant SO_2 flux.

H. PATIA[1, 2], S.M. EGGINS[2], R.J. ARCULUS[2], C.O. McKEE[3*], R.W. JOHNSON[4] AND A. BRADNEY[2]

1. RABAUL VOLCANOLOGICAL OBSERVATORY, P.O. BOX 3386, KOKOPO, PAPUA NEW GUINEA (DECEASED)
2. RESEARCH SCHOOL OF EARTH SCIENCES, AUSTRALIAN NATIONAL UNIVERSITY, CANBERRA, ACT 0200, AUSTRALIA
3. PORT MORESBY GEOPHYSICAL OBSERVATORY, P.O.BOX 323, PORT MORESBY, PAPUA NEW GUINEA
4. GEOSCIENCE AUSTRALIA, SYMONSTON, ACT 2601, AUSTRALIA

KEY WORDS: Rabaul Caldera - magma mixing - dacite - basalt - volatiles

* Corresponding author. Telephone: +675 3214500 E-mail: chris_mckee@mineral.gov.pg

Version of 26.08.17

ABSTRACT

The eruptions that began at Rabaul Caldera on 19 September 1994 had two focal points, the vents Tavurvur and Vulcan, located 6 km apart on opposing sides of the caldera. Vulcan eruptives define a tight cluster of dacite compositions, whereas Tavurvur eruptives span an array from equivalent dacite compositions to mafic andesites. The eruption of geochemically and mineralogically identical dacites from both vents indicates sourcing from the same magma reservoir. This, together with previously reported H_2O-CO_2 volatile contents of dacite melt inclusions, a caldera-wide seismic low-velocity zone, and a seismically active caldera ring fault structure are consistent with the presence at 3-6 km depth of an extensive, tabular dacitic magma body having volume of about 15-150 km^3. The Tavurvur andesites form a linear compositional array and have strongly bimodal phenocryst assemblages that reflect dacite hybridisation with a mafic basalt. The moderately large volume SO_2 flux documented in the Tavurvur volcanic plume (and negligible SO_2 flux in the Vulcan plume) combined with high dissolved S contents of basaltic melt inclusions trapped in olivine of Tavurvur eruptives, indicate that the amount of degassed basaltic magma was ~0.1 km^3 and suggest that the injection of this magma was confined to the Tavurvur-side (eastern to northeastern sector) of the caldera. Circumstantial evidence suggests that the eruption was triggered and evolved in response to a series of basaltic magma injections that may have commenced in 1971 and continued up until at least the start of the 1994 eruptions. The presence of zoned plagioclase phenocrysts reflecting older basalt-dacite interaction events (i.e. anorthite cores overgrown with thick andesine rims), evaluation of limited available data for the products of previous eruptions in 1878 and 1937-1943, and the episodic occurrence of major intra-caldera seismo-deformational events indicates that the shallow magma system at Rabaul Caldera is subjected to repeated mafic magma injections at intervals of several years to several decades.

INTRODUCTION

Background – geological context

The Rabaul Caldera Complex (RCC), located at the northeastern tip of the Gazelle Peninsula, New Britain Island, is one of the most active volcanic systems in Papua New Guinea having produced >35 km^3 of tephra during the past 20 ky (McKee et al., 2011). Over the longer term of the past 160 ky, the RCC experienced at least eight large (>5 km^3) ignimbrite-producing eruptions, some of which were caldera-forming (McKee and Duncan, 2016). This activity has contributed to the formation of the 15 × 10 km mostly sea-filled, nested caldera complex at Rabaul and to the creation of an extensive pyroclastic apron to the south and west (Nairn et al., 1995). The most recent caldera-forming eruption took place at 1400 BP and produced the >11 km^3 Rabaul Pyroclastics Formation (Walker et al., 1981; Nairn et al., 1995). Two other active volcanic systems are close neighbours of the RCC: the southeast-trending alignment of dominantly mafic stratovolcanoes, the Watom-Turagunan Zone (WTZ, Johnson et al. 2010), and the submarine caldera volcano Tavui (McKee, 2015), as shown in Figure 1. Detailed studies of the Rabaul area include those of geology and eruption history (Heming, 1974; Nairn et al., 1995; McKee et al., 2015, 2016; McKee and Duncan, 2016) and those of petrology and geochemistry (Heming and Carmichael, 1973; Heming, 1974, 1977; Wood et al., 1995). The work of Johnson et al. (2010) provides a synopsis and evaluation of the volcanic systems of the northeastern Gazelle Peninsula, and a general model for the active volcanism of the Rabaul area.

As shown in Table 1, historical records indicate the occurrence of at least six small-scale intra-caldera eruptions (<0.3 km^3) that took place at intervals of 24-59 years since 1767 when the navigator Philippe Carteret made the first record of observations of eruptive activity at Rabaul (Hawkesworth et al., 1773; Wallis, 1965). The three most recent eruptions,

WHICH STARTED IN 1878, 1937 AND 1994, INVOLVED SIMULTANEOUS ACTIVITY AT TWO VENTS, VULCAN AND TAVURVUR (FIG. 1), ON OPPOSITE SIDES OF THE CALDERA (BROWN, 1878; JOHNSON ET AL., 1981; FISHER, 1939; JOHNSON AND THRELFALL, 1985; BLONG AND MCKEE, 1995; JOHNSON ET AL., 1995; MCKEE ET AL., 2016).

The build-up to the 1994 outbreak of eruptive activity may have commenced in 1971 when seismicity and ground deformation within Rabaul Caldera began to intensify for the first time following the 1937-43 eruptions (Cooke, 1977; McKee et al., 1984, 1985; Mori and McKee, 1987; Mori et al., 1989; Itikarai, 2008). Locations of high frequency caldera earthquakes recorded since 1971 define an elliptical cylinder of seismicity that probably represents a ring fault associated with the current active caldera (Mori and McKee, 1987; Jones and Stewart, 1997; Itikarai, 2008; Fig. 1). Vulcan and Tavurvur lie about 1.5 and 1 km respectively outside of the surficial part of the zone of caldera seismicity. During the period 1983-1985 a phase of intense seismic activity and accelerated ground deformation occurred within the active caldera structure and an eruption was thought to be imminent. Two small magma bodies were initially inferred at 1-3 km depth from ground deformation data (McKee et al., 1984), but gravity and ground deformation data were subsequently interpreted to reflect a single magma body located at a depth of about 2 km under the central-southern part of the caldera (McKee et al., 1989). The volume of injected new magma thought to have been responsible for the seismicity and ground deformation during the period 1971-1985 was calculated to be of the order of 0.04 to 0.05 km^3 (McKee et al., 1984, 1989). Mori et al. (1989) suggested that both Vulcan and Tavurvur are fed from the sub-caldera magma body along radial and cone-sheet fractures, but Saunders (2001, 2006) and Itikarai (2008) favoured interpretations that involved magma movement within the ring fault and other fault structures prior to its emergence at the surface vents. Mori and McKee (1987) and Mori et al. (1989) noted the sharp cut-off of seismicity within the caldera at a depth of 4 km and interpreted this as the top of a larger magma body. Interpretation of data from a seismic tomography experiment conducted in 1997 (Rabaul

Earthquake Location and Caldera Structure – RELACS) has since defined a main region of anomalously low seismic velocity (interpreted as a magma body) between 3 and 6 km depth that is centrally located within the caldera and has lateral dimensions of 6 to 8 km (Finlayson et al., 2003; Bai and Greenhalgh, 2005; Itikarai, 2008). Other seismic low velocity anomalies were identified: one beneath the RCC in the depth range 9-18 km and another immediately north-northeast of the RCC at a depth of about 3 km within the WTZ (Bai and Greehalgh, 2005; Itikarai, 2008).

Caldera seismicity began to re-intensify in 1992 following an unusual swarm of earthquakes that took place about 2 km outside the northern part of the caldera seismic zone (Itikarai, 2008). The final phase of precursory activity commenced with two ~M5 earthquakes, one near Tavurvur and the other near Vulcan, at about 3 am on 18 September 1994 (GVN, 1994; McKee et al., 2017). The following 27 hours included a period of sustained strong caldera seismicity and massive ground deformation. Following the start of eruptive activity at about 6 am on 19 September 1994 seismicity on the ring fault decreased markedly to a very low level (Itikarai, 2008).

The eruptions that started in 1994

The eruptions that started at Rabaul in 1994 continued for many years but for convenience will be referred to as the "1994" eruptions. The eruptions can be divided into two phases: Phase 1 - September 1994 to April 1995; Phase 2 - late November 1995 onward. Detailed accounts and analysis of Phase 1 and parts of Phase 2 have been documented in GVN (1994), Blong and McKee (1995), Bouvet de Maisonneuve et al. (2015), McKee et al. (2016, 2017), and McKee (unpublished data). Eruptions at both sites produced identical dacites but the compositions of Tavurvur eruptives extended to mafic andesites.

Phase 1

At the beginning of Phase 1, which commenced on 19 September 1994, both Vulcan and Tavurvur were active. Vulcan's eruption was initially very powerful, involving periods of plinian activity that created a tall emission column, 18-30 km high, that led to the generation of numerous intra-caldera pyroclastic flows and locally very heavy falls of ash. A new cone complex was constructed on the northern side of the Vulcan headland. The total volume of ejecta was estimated to be about 260×10^6 m^3. Vulcan's eruption was short-lived, ending on 2 October 1994.

The eruption at Tavurvur was less powerful. At the peak of activity, during the first few days of the eruption, the emission column rose to about 6 km altitude and heavy falls of ash from Tavurvur emissions resulted in the collapse of many buildings in Rabaul Town. A small lava flow was emplaced on the western flank of Tavurvur in October 1994. Quasi continuous to intermittent (vulcanian) activity persisted at Tavurvur until April 1995. The total volume of ejecta was estimated to be about 40×10^6 m^3.

Phase 2

There has been no activity at Vulcan during Phase 2. Tavurvur's re-activation in November 1995 was the beginning of an extended period of activity, the latest episode of which was in August 2014. In general, Phase 2 has been characterized by intermittent mild (vulcanian) explosions. However, eight brief pulses of strombolian activity that produced spectacular fire fountains took place between May 1996 and August 1997. Substantial lava flows having a combined volume of about 14×10^6 m^3 were emplaced on Tavurvur's southern flank during four of the strombolian eruptions.

The strongest activity known from Tavurvur occurred in a burst of extremely powerful sub-plinian activity on 7 October 2006. The eruption column was maintained at about 18 km altitude for several hours and there were heavy falls of pumice lapilli and ash in a broad area around the vent. Partial collapse of the northwestern flank of Tavurvur resulted in the

formation of a debris flow. Lava effusion followed the structural failure and produced a broad-fronted lava flow, about 10×10^6 m^3 in volume, which covered Tavurvur's northern and western flanks.

The lastest episode of Phase 2 activity was a period of very powerful strombolian activity from Tavurvur that took place on 29 August 2014. A spectacular fire fountain was maintained for several hours and the eruption column reached an altitude of about 18 km.

This study

Analysis of the products of Phase 1 and those of Phase 2 until August 2001 is reported here. Existing brief accounts of the geochemistry and petrology of the initial phase of the eruption have highlighted the presence of hybrid andesitic magmas among volcanic products (Johnson et al., 1995; Roggensack et al., 1996). We have undertaken a detailed petrological and geochemical examination of the products of the 1994 eruption with the goal of establishing the nature of magmatic processes occurring at depth, both leading to and during the eruption. We also conducted a limited study of the petrology and geochemistry of the products of some earlier eruptions at Rabaul.

Sampling of 1994-2001 eruptives focussed on representative juvenile lava blocks/bombs and pumice clasts, lava flow fragments, and relatively coarse pumice lapilli (from the flanks and base of Vulcan and Tavurvur) so as to avoid compositional bias associated with winnowing of finer-grained fall deposits. Samples were collected from a month after the initial Phase 1 outbreak on 19 September 1994, and immediately following each significant eruptive episode during Phase 2 until August 2001. Three fine-grained ash samples were also collected, following explosive activity in May, July, and August 1999 as no lava/pumice blocks or coarse pumice lapilli were erupted during these events. Collectively these materials provide the basis for a detailed analysis of the temporal petrologic and geochemical evolution of the products of Phases 1 and 2 of the 1994 eruptions.

The principal author of this paper, Herman Patia, died in 2012. Herman spent his entire working life at Rabaul Volcanological Observatory (RVO) following his graduation from University of Papua New Guinea (UPNG) in 1985, and had become an identity in the international volcanological community. Herman contributed strongly to the programs of RVO, parts of which were pursued by Herman as research projects, resulting in awards of BSc (Honours) in 1989 for his work on Billy Mitchell Volcano, Bougainville, and M. Phil. in 2004 for his work on the products of the 1994-2001 eruptive period at Rabaul. Herman's M. Phil study forms the basis of this paper. At the time of his death, the manuscript of this paper was well advanced. We, the co-authors, believe that by bringing this work to publication, Herman's legacy will be enriched.

PETROGRAPHY AND MINERALOGY

Methods

Crystals, melt inclusions and matrix glasses were analysed in representative samples by energy dispersive techniques using Camebax and Jeol electron microprobes operating at 15kV accelerating voltage and 1-5nA beam current. Crystal compositions have been systematically characterised, including the analysis of core and rim compositions, in 30 thin sections. The compositions of the principal phases (plagioclase, pyroxene, and olivine) in the Vulcan and Tavurvur Phase 1 and 2 samples are summarised in Figures 3 and 4.

Petrography

Pumice blocks and ash erupted from Vulcan in Phase 1 are typically pale grey to grey or tan-grey in colour. Crystal assemblages in these materials are dominated by small to moderately large (up to ~5 mm) euhedral plagioclase (~10 vol.% vesicle free), with minor amounts of clinopyroxene (1-2 vol.%), orthopyroxene (1-2 vol.%), magnetite (0.5 vol.%), and a trace of olivine. Clinopyroxene and orthopyroxene are characteristically small (≤1mm) and relatively equant in shape, and occur commonly in glomerophyric clusters with magnetite and plagioclase (Fig. 2A). All crystals are euhedral and have no obvious dissolution features. Accessory apatite needles and sulphide blebs are included in plagioclase and in magnetite respectively. Glassy and devitrified melt inclusions are common in plagioclase and other crystalline phases. The groundmass is typically microcrystalline, but light brown glass patches occur among crystal clusters. The microcrystalline groundmass could imply shallow decompression crystallization prior to eruption. Alternatively this may be a product of undercooling due to mixing across a curved cotectic (as per Gerlach and Grove, 1982).

Blocks and lavas erupted from Tavurvur in both Phase 1 and Phase 2 are characteristically dark grey but range from light grey to jet-black in colour. They occasionally display cm-scale colour variation banding that is observed in thin section to correspond to regions of different

groundmass crystallinity. Many samples contain abundant, sometimes large (> 5 mm), crystals of plagioclase (up to 25-28 vol.% vesicle free) and variable amounts (<0.5-5 vol.%) of relatively coarse-grained olivine (1-3 mm, Fig 2B) and clinopyroxene (1-5 vol.%). A population of smaller sized crystals of clinopyroxene and orthopyroxene (1-3 vol. %), magnetite (0.5-3 vol. %), accessory apatite and occasional sulphides (<0.5 vol. %), similar to that observed in Vulcan dacites are also present. Glomerocrysts and clots of medium to coarse-grained plagioclase, clinopyroxene and olivine are a feature of samples that are richer in olivine and clinopyroxene. Clinopyroxene and olivine are characterised by weak to absent optical zoning. Plagioclase is invariably euhedral, complexly zoned and typically contains abundant glass inclusions within cores. The latter are occasionally overgrown by largely melt inclusion-free and oscillatory-zoned rims (Fig. 2D). Accessory apatite needles and rods are common, particularly as inclusions in sodic plagioclase (Fig. 2C and D). The groundmass is invariably microcrystalline, except for the occurrence of light to dark brown matrix glass patches within crystal aggregates.

Mineral compositions

Plagioclase crystals in Vulcan samples are dominated by labradorite compositions (An_{65-45}) but extend to very anorthite-rich compositions (An_{95}; Fig. 3). Ferromagnesian phases are characterised by relatively Fe-rich clinopyroxene (Mg_{76-72}), orthopyroxene (En_{75-69}), homogenous olivine (Fo_{79-78}) and titanomagnetite with 8-12 wt% TiO_2. In contrast, Tavurvur Phase 1 and 2 samples typically have strongly bimodal crystal contents. One mode comprises crystal compositions that generally overlap with those present in Vulcan dacites including a similar range and distribution of plagioclase compositions, relatively Fe-rich augitic clinopyroxene (Mg_{77-72}), orthopyroxene (En_{74-68}) and zoned olivine (Fo_{79-69}). The other mode is characterised by magnesian clinopyroxene (Mg_{86-82}), olivine (Fo_{86-80}) and calcic plagioclase (An_{97-85}); this assemblage is prevalent in the most mafic samples (Fig. 5a-c). Coexisting Fe-

rich clinopyroxene and orthopyroxene occur in Vulcan samples and in Tavurvur Phase 1 and 2 samples. Compositions cluster on and between the 950-1050°C isotherms of the graphical geothermometer of Lindsley (1983; Fig. 4).

Paired analyses of plagioclase cores and rims reveal a complex crystalline assemblage dominated by a population of relatively unzoned labradorite (An_{50-60}) and another group of unzoned calcic plagioclase (An_{85-95}), a few reversely zoned crystals and a large population of normally zoned crystals which have core compositions ranging from labradorite to anorthite (An_{50-90}) with labradorite (An_{50-60}) rims (Figs. 5 and 6). Compositional profiling from core to rim and element mapping by electron microprobe reveals the latter normally-zoned crystals typically have sharp boundaries between their calcic cores and sodic overgrowths, consistent with petrographic observations.

WHOLE-ROCK GEOCHEMISTRY

Methods

One hundred and twenty four samples from the 1994 to 2001 eruptive period were analysed for whole-rock major and trace elements by X-ray fluorescence at the Australian National University and Geoscience Australia following the methods of Norrish and Hutton (1969) and Norrish and Chappell (1977). A subset of samples was analysed for rare earth elements (REE), other trace and minor elements by solution nebulisation inductively coupled plasma source mass spectrometry (ICPMS) and by laser ablation (LA) ICPMS at the Australian National University using the methods of Eggins et al. (1997) and Eggins (2003). Preparation of samples for analysis involved removal of surface coatings prior to jaw crushing and pulverising to a fine powder in a tungsten carbide ring mill. The sample powders were fused (1:10 ratio) with a 12:22 lithium-tetraborate/metaborate mixture (Sigma Chemicals 12:22 flux) and quenched as glass discs for major element analysis using Phillips PW1400 and PW1400a spectrometers. Powder pellets were pressed in Al cups for trace element analysis using wavelength dispersive (Phillips PW1440) and energy dispersive (Spectro-Lab XRF) spectrometers. Representative analyses that encompass the compositional range of Vulcan and Tavurvur Phase1 and Phase 2 eruptives are listed in Table 2.

Chemical compositions

The analysed samples form a continuous linear array from 58 wt% to 63 wt% SiO_2 straddling the boundaries between high-silica andesite and low-silica dacite, and medium-K to high-K compositions (Fig. 7; after Gill, 1981). The 1994-2001 eruptives are generally concordant with the compositions of historical and prehistorical Rabaul eruptives (Wood et al., 1995), which form an array from high-alumina basalt to rhyodacite compositions (Fig. 7).

The major and minor oxide compositions of the 1994-2001 eruptives and previously analysed Rabaul samples have been plotted against MgO in Figure 8. A striking feature of the 1994-

2001 data is the tight linear trends on all of these plots. The low-MgO end of the 1994-2001 data set is defined by the Vulcan 1994 dacite compositions and a cluster of virtually identical Tavurvur Phase 2 dacites having 1.8-2.1 wt% MgO; these correspond fairly closely with dacite compositions erupted in 1937 and 1878. The trend toward more MgO-rich compositions is defined only by Tavurvur samples, particularly those from Phase 2, which extend to magnesian andesites having up to 4.5wt% MgO.

The compositional trends for major elements formed by the 1994-2001 eruptives diverge from and are distinct from the compositional arrays of most previous Rabaul eruptives (Fig. 8). Few andesite compositions matching those erupted in 1994-2001 have been reported previously from Rabaul. Studies by Wood et al. (1995) and by Heming (1977) have argued that the compositions of historical and prehistorical eruptives are consistent with magma evolution by fractional crystallisation. Both petrographic observations and compositional variation trends for historical and prehistorical eruptives are consistent with initial olivine, clinopyroxene, and plagioclase fractionation, joined later by Ti-magnetite saturation (evidenced by inflection at ~3 wt% MgO as shown in Fig. 8e; see also Heming, 1977). The hump of high Al_2O_3 compositions in prehistorical eruptives, >19-20 wt% (Fig. 8b), we attribute to plagioclase accumulation. The onset of orthopyroxene crystallisation is not associated with any compositional inflection but is consistent with the overall melt evolution trajectories required by least squares modelling to account for the evolution of observed dacites from andesitic parent compositions (Wood et al., 1995; Heming, 1977). Apatite fractionation occurs only in dacite compositions as indicated by the distinct inflection in P_2O_5 at ~1.8 wt% MgO (Fig. 8h).

Selected trace element abundances are plotted versus MgO wt% in Figure 9. As with the major and minor oxides, trace element abundances for the 1994-2001 samples form tight linear correlations that diverge from prehistorical compositions having higher MgO contents. The highly compatible elements Ni and Cr form steeply increasing, near-linear positive correlations with increasing MgO; moderately and variably compatible elements (V, Cu, and Sr) form less

steeply increasing trends; and the highly incompatible elements (Rb, Zr and Ba) form steeply decreasing, near-linear correlations with increasing MgO. These systematics are consistent with the behaviour of petrogenetically-linked major oxides. For example, the almost flat trends observed in 1994-2001 eruptives for Sr and Al_2O_3, both of which are compatible in plagioclase, contrast with the increasing trends of Sr and Al_2O_3 observed in prehistorical eruptives with <5wt% MgO. Likewise, the incompatible trace elements and major oxides (Na_2O, K_2O and P_2O_5) all decrease less steeply with increasing MgO in 1994-2001 eruptives compared to the groupings of older eruptives.

Temporal variations in magma composition

A plot of MgO wt% as a function of time through the 1994-2001 period of activity (Fig. 10) illustrates an increased spread of magma compositions from the beginning of Phase 1 (Sept. 1994) until well into Phase 2 (early 1998). The most MgO-rich compositions were erupted during the eight periods of strombolian activity (May 1996 to August 1997), subsequent to which relatively low MgO (2-2.5 wt%) compositions only were erupted. It is notable that dacites with low MgO (1.8-2.1 wt%) were interspersed with more-magnesian andesite compositions throughout the course of the eruption, and often in the same eruptive event. The minimum MgO content of the dacites appears to increase steadily from about 1.8 to 2.0 wt% MgO through the eruption (Fig. 10).

Products of the 1878 and 1937-43 eruptions

Thirty eight samples from the products of recent historical eruptions were collected as part of this study and related previous work (Patia, 2003): seventeen samples from 1878 eruptives and twenty one samples from 1937-43 eruptives. Mineralogical examination and electronprobe analyses of mineral chemistry of the 1937-43 samples reveal bimodal phenocryst assemblages similar to those of the 1994 eruptives. The Tavurvur 1937-43 eruptives have bimodal populations of relatively unzoned plagioclase phenocrysts with broadly anorthite (An_{85-95}) and

andesine to labradorite (An_{45-65}) compositions. Equivalent Vulcan eruptives show dominant andesine to labradorite (An_{45-65}) compositions and some highly anorthite-rich phenocrysts associated with mafic micropillows containing highly magnesian olivine (Fo_{90-91}). The 1878 eruptives of both Tavurvur and Vulcan show a less extreme range of plagioclase compositions dominated by a population of unzoned labradorite (An_{50-60}) and lesser bytownite (An_{70-80}), and other normally zoned phenocrysts that span the same compositional range (Patia 2003).

Representative geochemical analyses of a sub-set of these samples were presented by Patia (2003). In general, these analyses are similar to those of products from the 1994-2001 period of activity, however some highly magnesian analyses (5.4-8.2 wt% MgO) were obtained for some relatively rare products of both the 1878 and 1937 Vulcan eruptions (see Figures 8 & 9). The MgO contents of the bulk of the 1878 and 1937-43 eruptives show less variation than the products of the 1994 eruption: the MgO range for most 1878 eruptives is 1.6 to 2.3 wt%, while the principal 1937-43 products have a slightly broader range, 1.4 to 2.6 wt% MgO (Fig.10).

DISCUSSION

Magma interaction and mixing as shown by eruptive products of the period 1994-2001

The strongly bimodal phenocryst populations and tight rectilinear compositional variation trends formed by the 1994-2001 eruption products are *prima facie* evidence for mixing of two distinct magmas. The two magmas involved are both crystal-bearing and include a dacite with ~1.8 wt% MgO and 64 wt% SiO_2, and a less well constrained, more-mafic magma that has >4.5 wt% MgO. It is particularly significant that evidence for eruption of the same dacitic magma, with its characteristic bulk composition and crystalline phase assemblage (plagioclase An_{65-45}, augite clinopyroxene Mg_{77-72}, orthopyroxene Mg_{75-68}, titanomagnetite, apatite and sulphide), is present at both Vulcan and Tavurvur, on opposite sides of the caldera. While we can also identify a mafic phenocryst assemblage within the andesite-dacite samples that cannot have been in equilibrium with dacitic melts, a mafic magma containing only this phenocryst assemblage has not been sampled.

Figures 8 and 9 show that the relatively MgO-rich andesites erupted from Tavurvur have no correlatives with previously erupted and analysed Rabaul rocks. However, the 1994-2001 andesite compositions are not necessarily exotic in the Rabaul context, as extrapolation of the linear trends formed by this sample set project to plausible high-MgO basalt parental magma compositions having 8-10 wt% MgO (see Fig. 8). It is possible that the mafic end-member of the 1994-2001 eruptive sequence is a MgO-rich basalt, which has been mixed with dacite in proportions as high has 55:45 (if 8 wt% MgO) or 30:70 (if 10 wt% MgO) to form the most magnesian andesite compositions erupted in Phase 2. If so, it follows that the mafic magma was relatively crystal-rich, given the significant modal abundances of calcic plagioclase (8%), magnesian olivine (5%) and magnesian clinopyroxene (3%) observed in the most magnesian Tavurvur andesites (Patia, unpublished data). This is consistent with the composition of olivine-hosted basaltic melt inclusions in 1994 Tavurvur andesites, which have high-Al basalt

compositions clustering between 4 and 4.5 wt% MgO, and as high as 4.9 wt% MgO (Roggensack et al., 1996, Fig. 10). We suggest on this basis, together with the lack of zoning in magnesian clinopyroxene phenocrysts which might otherwise be expected to record cores grown from more magnesian melt compositions, that the highly magnesian (likely 8-10 wt% MgO) nature of the mafic magma is due to the accumulation of significant quantities of magnesian olivine and clinopyroxene phenocrysts.

Depth and extent of magma bodies

The sub-caldera dacitic magma body at Rabaul interpreted from the results of seismic tomographic imaging has lateral dimensions of about ~6-8 km and thickness of ~3 km (Finlayson et al., 2003; Bai and Greenhalgh, 2005; Itikarai, 2008). This thickness may be regarded as an upper bound due to tomographic smearing effects, with the true thickness being possibly of the order of 0.5 km or less. Thus, the volume of the interpreted magma body is estimated to lie in the range ~15-150 km^3, although a portion of this volume may be only partially molten.

The shallow depth of the magma body inferred from tomography is consistent with the relatively low H_2O contents (2.0-2.3 wt%) of plagioclase-hosted, dacitic melt inclusions reported from the Phase 1 part of the eruption (Roggensack et al., 1996). Similar low H_2O contents were determined for plagioclase-hosted dacitic melt inclusions in the products of the 2006 eruption (Bouvet de Maisonneuve et al., 2015). This amount of H_2O corresponds to the water solubility limit in siliceous melts at ~50 Mpa and to the estimated lithostatic load at a depth of ~3 km (Roggensack et al., 1996). The dacite magma was almost certainly volatile-saturated prior to eruption, as evidenced by the relatively uniform H_2O content of the dacitic melt inclusions.

The basaltic recharge magma may have been somewhat deeper than the dacitic magma body when olivine crystallization commenced. Roggensack et al. (1996) reported 2.8-3.8 wt% H_2O

and variable CO_2 contents (<50-960 ppm) in basaltic, olivine-hosted melt inclusions from the Phase 1 Tavurvur andesites. The H_2O and CO_2 contents of these melt inclusions correspond to solubility limits in basaltic magmas spanning a pressure range from <150 to 250 MPa, and indicate olivine crystallisation occurred at depths greater than ~5-9 km. This is significantly deeper than crystallisation of the dacite magma (i.e. ~3 km), and indicates entry of mafic magma into the shallow dacitic magma reservoir from below, as concluded by Roggensack et al. (1996). Given that Rabaul dacite may evolve from basalt and basaltic andesite parental melts by between 60 and 75% fractional crystallisation (Wood et al., 1995), then potentially ≥70% of the dissolved magmatic H_2O is lost during differentiation (basalt to dacite) through exsolution of a H_2O-rich magmatic volatile phase.

The synchronous eruption of compositionally and mineralogically identical dacite magmas at Vulcan and Tavurvur during the 1994 eruption implies that these vents, on opposing sides of the caldera, tap a common magma reservoir. This conclusion is reinforced by the synchronous eruption from both Vulcan and Tavurvur of similar dacite compositions in 1878 and again in 1937-43. This indicates the persistence of a common dacitic magma body for at least 120 years (and probably much longer). Subtle differences exist between the common end-member dacitic magma compositions erupted in 1878, 1937-43, and 1994-2001. The end-member dacite erupted in 1878 has 1.71 ± 0.05 wt% MgO, which decreases to 1.63 ± 0.06 wt% in 1937, and then increases again to 1.86 ± 0.06 wt% in 1994-2001. These changes indicate that the dacitic magma body undergoes compositional evolution between eruptions that involve both fractional crystallisation and addition of more-mafic magmas. Least squares modelling using observed phenocryst assemblages and phase compositions reveals that the decrease from 1.71 wt% MgO in 1878 to ~1.63 wt% MgO in 1937 requires between 4 and 5 mass % fractional crystallisation of the 1878 dacite magma over a period of 59 years (see Table 3). Given the estimated volume range for the magma reservoir, ~15-150 km^3, we suggest an estimated corresponding volume of magma that crystallised over the period 1878-1937 to lie in the range 0.6 to 7.5 km^3. This

estimate does not acknowledge that a portion of the low-velocity region is probably only partially molten.

Volume of injected mafic magma

The volume of injected mafic magma may be estimated by consideration of the SO_2 yield. TOMS (Total Ozone Mapping Spectrometer) and airborne COSPEC (correlation spectrometer) measurements (GVN, 1994; Roggensack et al., 1996) recorded moderate SO_2 contents in Tavurvur's September 1994 eruption plume but no detectable SO_2 in Vulcan's plinian eruption column, indicating degassing of a S-rich melt, and hence basalt injection, beneath and through Tavurvur but not Vulcan (Roggensack et al., 1996). Analyses of olivine-hosted melt inclusions from the Phase 1 and early Phase 2 products of Tavurvur indicate that the most primitive basaltic andesite and basaltic compositions (with > 4 wt% MgO) have S contents in the range 1800 ± 120 ppm whereas dacite composition matrix glass and melt inclusions contain <120 to 400 ppm S (Roggensack et al., 1996). The total SO_2 yield during the first 18 days of Tavurvur's eruption in 1994 was about 500 ktons, released at rates that declined from 30-80 ktons/day in the first few days to 26 ± 5 ktons/day on day 10, and to 4 ± 1 ktons/day by day 18 (see Fig. 1 in Roggensack et al., 1996). Assuming that the total SO_2 yield was derived from degassing of a new basaltic magma injection upon ascent, we estimate the mass of fresh injected basalt to be 1.4×10^8 tons (equivalent to ~0.06 km^3). Note that the mass calculation and volume estimate from gravity measurements during the period 1973-1985 were 1×10^8 tons and 0.04 km^3 (McKee et al., 1989). Given the S content of the erupted matrix glass remained significant (i.e. at ~100-200 ppm; Roggensack et al., 1996), and the bulk S content of the mafic magma was probably less than 1800 ppm due to dilution by abundant phenocrysts, a larger volume approaching ~0.1 km^3 may be a more reasonable estimate. This would represent only 0.07-0.7% of the estimated volume of the magma chamber, 15-150 km^3. It is however significantly larger than the volume of mafic magma entrained in the Tavurvur andesite-dacite

eruptives (<0.02 km^3 based on mass balance if the mafic magma end-member is assumed to have >5.5 wt% MgO).

Mafic magma injection - cause of eruption?

It is plausible that a series of injections of basaltic magma into the dacite magma reservoir resulted in sufficient temperature increase and overpressure to cause instability of the shallow dacite-filled reservoir. No seismic or other activity can be linked unambiguously to the ascent of magma from depth in the period immediately prior to commencement of the 1994 eruptions. The two ~M5 earthquakes recorded 27 hours prior to the eruption (GVN, 1994; McKee et al., 2017) occurred at shallow depth (1-2 km) near Tavurvur and Vulcan and probably reflect rupture that initiated magma ascent from the caldera-extensive reservoir possibly triggered by mafic magma recharge. Simple models for magma chambers located beneath shallow volcanic piles indicate that the overpressure needed to induce wall-rock rupture is of the order of 1-10 Mpa (Blake, 1981; Tait et al., 1989). The overpressure produced by injection of new magma into an existing chamber is a function of the relative volumes and the compressibility of the new and resident magmas, and of the elasticity of the wall-rock (Blake, 1981). An injected/resident magma volume ratio exceeding 0.001 will cause failure of a reservoir filled with incompressible magma, but this can increase to ~0.01 if the resident magma contains a compressible magmatic volatile phase. Where pre-existing magma or fluid-filled fractures emanate from a magma chamber relatively small overpressures and significantly reduced injected/resident magma volume ratios may lead to dyke growth from magma reservoirs (McLeod and Tait, 1999). In this case magma viscosity exerts fundamental control upon the rate at which these dykes propagate.

Given the volume of injected mafic magma was of the order of ~0.1 km^3 (based on the SO_2 yield in Phase 1, see above) and assuming that the Rabaul dacitic magma was volatile-saturated (Roggensack, et al., 1996) and pre-existing magma-filled fractures were absent, the likelihood

of magma reservoir failure and subsequent eruption in 1994 would have been greater if the magma reservoir volume was nearer to the lower end of the estimated range, i.e. ~15 km^3. This assumes that the entire mafic magma injection was needed to exceed the failure threshold and is notable as the interpreted injection of a similar volume of new magma during the 1983-1985 seismic crisis (McKee et al., 1989) did not result in eruption. Thus, it seems plausible that repeated basaltic magma injections took place during the 23 years period of volcanic unrest (Johnson et al., 2010) and had a cumulative effect of pushing the system beyond the failure threshold in 1994.

Phase 2 activity – possible implications of repeated mafic magma injections

The 1994-2001 period of eruptive activity and the previous eruption (1937-43) are notable for the synchronous eruption of Vulcan and Tavurvur, and for volcanic activity occurring at Tavurvur over a period of years following the initial eruption. Unlike previous eruptions, considerably more mafic material is present in the 1994 eruption products, particularly during the early parts of Phase 2. The basaltic magma component documented in both Phase 1 and Phase 2 is mineralogically and compositionally identical, suggesting that the initial and subsequent phases of volcanic activity over the period 1994-2001 are an outcome of repeated injections of the same or similar basaltic magma. These injections may have started in 1971. We further speculate that the basalt formed a dense basal layer that was restricted to the eastern-northeastern side of the existing broad shallow dacite-filled magma reservoir. Relatively rapid heat exchange between the magmas would induce crystallisation and accompanying volatile exsolution from the basaltic magma over a period of months or years prior to reaching thermal equilibrium with the overlying dacite magma, before overturn of the mafic and silicic layers dispersed and mixed the injected basalt into the dacite (as per Snyder, 2000). During this period of slow cooling, hybridisation of the basaltic and dacitic magmas may have occurred at their interface due to convective entrainment of the basalt within the

thermal boundary layer of the dacite. In addition, volatile exsolution from the mafic magma may have resulted in formation and ascent of buoyant (bubble-rich) plumes into the overlying dacite. Such processes might account for the trend of increasingly mafic erupted dacite compositions, from ~1.86 to >2.0 wt% MgO, over the course of the 1994-2001 eruptive period. The eruption of variably more mafic andesites in both Phase 1 and Phase 2 requires only partially complete hybridisation processes. More detailed petrologic examination of the Phase 1 and 2 products, particularly the evolution of matrix glass compositions, may illuminate these and other aspects of the basalt/dacite magma hybridisation processes that took place.

Comparison with previous eruptions

The MgO-rich andesites and extended magma mixing trends that characterise the 1994-2001 eruptive period have not been documented previously at Rabaul (c.f. Wood et al., 1995). This could indicate that the 1994-2001 activity is an atypical event or, alternatively, that evidence for magma mixing/mingling and hybridisation may have been overlooked in the products of earlier eruptions. Discriminating between these possibilities is critical to understanding how the Rabaul magma system works, particularly if mafic magma injections have played a key role in past eruptions in a manner similar to that implicated for the 1994 eruptions. Drawing on more recent data acquired for historical eruptions (Patia, 2003) we conclude that substantial evidence exists for mafic magma injections and interaction between mafic and felsic magmas in previous eruptions. This includes significant variations in the MgO contents of erupted magmas (Fig. 10), the occurrence of bimodal phenocryst assemblages and zoned plagioclase phenocrysts, and textural evidence of magma mixing/mingling in the products of the 1878 and 1937-43 eruptions. The more mafic dacite compositions (~1.86 - >2.0 wt% MgO) erupted in 1994-2001 compared with those of 1937-43 (~1.63 wt% MgO) are consistent with the addition of mafic magma to the dacite magma reservoir subsequent to the 1937-43 eruption, and may be linked to the onset of volcanic unrest in 1971, the 1983-85 seismo-deformational crisis (Mori et al., 1989), the resurgence of seismicity in 1992, the beginning of the 1994 eruptions and during the

1994-onwards eruptive period. We also note the common occurrence in the 1994-2001 Vulcan and Tavurvur dacites of plagioclase phenocrysts with variably thick sodic overgrowths, which have grown in equilibrium with dacitic magma, over 'older' cores crystallised in equilibrium with basaltic magma. These observations lead us to conclude that mafic magma injections have occurred repeatedly into a 'long-lived' shallow dacitic magma reservoir and that these injections may also be responsible for triggering eruptions at Rabaul. Detailed studies of the products of historical and prehistorical eruptions using newly developed chronometers that are able to constrain the timescales of magma mixing prior to eruption (e.g. Costa et al., 2008) are needed to further test this important hypothesis.

The contrast between the compositional patterns displayed by the whole-rock elemental data for the 1994 eruption products and data from many previous eruptions, particularly prehistorical events, as shown in Figures 8 and 9, is intriguing. This may suggest that different processes from those associated with the 1994 eruptives acted throughout much of the history of the RCC and WTZ systems. Limited data for the 1878 and 1937-43 eruptives, particularly the high-MgO analyses which appear to lie on an extension of the compositional trend for 1994 eruptives (Figs. 8 & 9), suggest similarity of the magmatic processes that operated through the recent historical period.

Accumulation of phenocrysts may be a common process at both the RCC and WTZ systems. We have suggested that the accumulation of plagioclase explains the finding of high Al_2O_3 at high MgO in prehistorical eruptives. This process would also be consistent with evidence of high CaO and high Sr at high MgO, although accumulation of pyroxenes would also contribute to the high values of CaO. Accumulation of olivine and pyroxenes would be consistent with high Fe_2O_3 at high MgO. Phenocryst accumulation also took place prior to the 1994 (and other historical) eruptions as magmatic end-members in each case were crystal-enriched and there is evidence of different generations of crystallization and reaction to changing magmatic compositions. However, the different evolutionary trajectories of the whole-rock elemental

data for the 1994 and other historical eruption products compared with data from previous eruptions may indicate differences in phenocryst accumulation processes over time or the operation of other (currently unknown) processes in either the historical or prehistorical period.

Comparison with other studies of magma mixing/mingling as an eruption trigger

In the words of A.T. Anderson (1976) "magma mixing is a widespread, if not universal igneous phenomenon", and is regarded as a common mechanism for triggering explosive eruptions of felsic magmas (Sparks et al., 1977). Extensive and efficient mixing produces hybridized magmas that have disequilibrium mineral assemblages and characteristic mineral textures and crystal zoning (eg. Streck, 2008), whereas less-efficient mixing (mingling) results in disintegration of one interacting magma and the incorporation of fragments (inclusions) of that magma in the other interacting magma. A number of models have been proposed to address the range of outcomes produced by variations in the extent of mixing and mingling, e.g. the "foam-instability" models of Eichelberger (1980) and Thomas and Tait (1997), and the "pillows" model of Huppert et al. (1982). The array of hybridized andesites produced at Rabaul in the period 1994-2001 represents relatively efficient mixing of dacite and basaltic magmas. Similarly efficient mixing, involving basalt and andesite, took place at Karymsky in 1996 (Izbekov et al., 2002, 2004). At the other end of the mixing scale, the products of Soufriere Hills in 1995-1999 (Murphy et al., 1998, 2000), showing ubiquitous coherent inclusions of mafic material within andesite, represent magma mingling. Strong textural evidence of mingling of andesite and rhyolite is shown by the 2000 BP products of El Misti (Tepley et al., 2013). Intermediate and variable degrees of mixing and mingling are represented by the products of Pinatubo 1991 (Pallister et al., 1996) and Lassen Peak 1915 (Clynne, 1999). Four different magmatic components are present in the products of Pinatubo 1991: phenocryst-rich and phenocryst-poor dacite, olivine-clinopyroxene-hornblende basalt, and hybrid andesite. The basalt occurred as undercooled and quenched inclusions in the hybrid andesite. Similarly, four different rock types were produced at Lassen Peak in 1915. Complex mixing involved variable

degrees of disaggregation of inclusions of undercooled andesite within hybrid dacite. The glomerocrysts and clots of plagioclase, clinopyroxene and olivine in magnesium-rich samples of the early products of Tavurvur in 1994 (Johnson, et al., 1995) signify less efficient mixing, possibly representing an earlier recharge event.

The mafic component of mixed-magma eruptions is commonly not erupted as a discrete entity (Sparks et al., 1977). This was the case for Rabaul's 1994 eruptions where the basalt end-member was never sampled despite the flux of basalt at Rabaul being greater in 1994 than in the previous eruptions (1937-43 and 1878). This variation has similarities to the increased flux of basalt at Mount St Helens over the last 4 ky (Gardner et al., 1995). As noted by Cashman et al. (2017) mixing of successive recharge batches of mafic magma with felsic magma may be quite efficient, resulting in the ubiquity of antecrysts and glomerocrysts, although mafic enclaves (micropillows) are occasionally preserved, as in the 1937 Vulcan eruptives (Patia, 2003).

Non-eruptive recharge events may be common. At Rabaul there are seismic indications of recharge starting in 1971, a strong pulse in 1983-1984, another pulse in 1992, and a possible recharge event immediately prior to the outbreak of the eruptions. A similar scenario has emerged at Soufriere Hills where multiple recharge events are indicated by a series of seismic swarms at intervals of about 30 years prior to the 1995-1999 eruption (Murphy et al., 1998, 2000). While seismicity may be equivocal as evidence for recharge, mineralogical evidence is more compelling. In the case of El Misti 2000 BP multiple recharge events are indicated by two populations of andesite-sourced amphibole within rhyolite – with and without reaction rims (Tepley et al., 2013). The amphibole phenocrysts that have reaction rims represent earlier non-eruptive recharge events that were not linked directly to the eruption-triggering process at 2000 BP. The "Minoan" caldera-forming eruption of Santorini in the late 1600s BC also was preceded by several non-eruptive mixing events during a period of perhaps 100 years (Druitt et al., 2012).

Where magma recharge leads directly to eruption the time interval for this process may be of short duration, perhaps hours in some cases, and commonly only days. An immediate response to a regional basaltic dyke injection is indicated by the simultaneous eruptions in 1996 of basalt at Academy Nauk caldera and basalt-triggered andesite at the neighbouring Karymsky (Izbekov et al., 2002, 2004). At Rabaul in 1994 the final recharge event may have been linked with the two M5 caldera earthquakes only 27 hours prior to eruption outbreak. Similar time periods between eruption-triggering recharge and actual eruption are indicated for Arenal (Coombs and Gardner, 2004) and Mount Hood (Kent et al., 2010). A time period of about one month separated the onset of mixing of andesite and dacite and the eruption outbreak at Southwest Trident in 1953 (Coombs et al., 2000). For the 1991 Pinatubo eruptions, basalt began to leak into a crystal-rich dacite reservoir about two months prior to the series of magmatic eruptions (Pallister et al. 1996). However, a larger or more violent episode of mixing, associated with intensified deep long-period earthquakes that started about one week prior to the onset of the magmatic eruptions (White, 1996), may have initiated the processes that led to the climactic eruption (Pallister et al., 1996).

A model for the Rabaul-region magma systems

A general model for the volcanism at Rabaul must accommodate the multiplicity of local magma systems, the possibilities of interaction between these systems and the evidence of basaltic recharge at the RCC. The Rabaul region hosts three magma systems, individually associated with Rabaul Volcano, the WTZ and Tavui Volcano. Petrological relationships link the eruptive outputs from the Rabaul system and those from the WTZ (Wood et al., 1995), but contrasts between the geochemical and mineralogical characteristics of the higher-K Rabaul-WTZ “main series”, which is quartz-free and lacks hydrous minerals (Wood et al., 1995), and the lower-K Tavui rock series, that contains quartz and hornblende (Wallace and Tufar, 1998), indicates independence of the Tavui system. The mafic end-members of each of the Rabaul and Tavui rock series are similar to the principal products of the WTZ, while the felsic end-

member of the Rabaul system is rhyodacite and Tavui's felsic end-member is rhyolite (Wood et al., 1995; McKee, 2015).

The model presented here for the Rabaul-area magma systems builds on an earlier model (Johnson et al., 2010) and invokes the concept of complex, vertically-extensive and unstable magma storage regions from mantle to crust in a transcrustal magma system (TCMS, as proposed by Cashman et al., 2017). Mantle-derived basalt is the starting material for all three magma systems of the Rabaul area (Fig. 11). Storage (underplating) and fractionation may occur at the base of the crust where lateral movement of magma may be possible and some crustal melting may take place. For the caldera systems, mid-crustal storage and fractionation is envisaged to provide more-evolved magmas to upper crustal magma bodies. The Rabaul sub-caldera dacite body is shallow and permanent due to a high rate of recharge (c.f. Sparks et al., 1977). The high recharge rate and relative frequency of eruptions limit the felsic end-member composition to rhyodacite (Wood et al., 1995; McKee, 2015; McKee and Duncan, 2016). A sub-caldera magma body at Tavui may be somewhat deeper than the corresponding entity at Rabaul as suggested by the appearance of amphibole in felsic eruptives from Tavui (Wallace and Tufar, 1998), and may be ephemeral. The failure of geophysical imaging techniques to confidently detect a shallow crustal magma body beneath Tavui (e.g. Finlayson et al., 2003) may be consistent with the difficulty of maintenance of such magma bodies in some cases (Cashman et al., 2017). A suspected low rate of magma recharge and an apparently low frequency of eruptions would provide conditions conducive for Tavui magmas to reach their full felsic potential, i.e. rhyolite. Upper crustal storage and fractionation takes place within the WTZ system (Johnson et al., 2010). Eruptions from the Rabaul system may be the culmination of repeated mafic (or less felsic) injections from below, and possibly laterally also, from the WTZ (Johnson et al. 2010). There is no evidence for pre-eruptive contact between mafic magma from the WTZ and felsic magma from Tavui, however the sequential eruptions at 6.9 ka BP of basaltic Raluan Scoria from a WTZ vent (Nairn et al., 1995) and rhyolitic Raluan

Ignimbrite, arguably from Tavui (Wallace et al., 2002; McKee, 2015), suggests some form of interaction between these systems in this instance. More-detailed work on the products of all three magma systems of the Rabaul area will test and refine this general model of local igneous processes.

CONCLUSIONS

1. Whole-rock geochemical data and phenocryst mineral chemistry indicate the eruption of identical dacitic magmas from the vents Vulcan and Tavurvur, on opposite sides of Rabaul Caldera, and provide evidence for tapping of the same caldera-extensive dacitic magma reservoir by both vents.

2. Hybridised andesitic magmas having strongly bimodal phenocryst assemblages and forming a linear compositional array that extends from end-member dacite toward a mafic basalt composition were erupted from Tavurvur during both phases of the 1994-2001 eruptive period and are interspersed with dacites. The linear compositional array formed by the Tavurvur eruption products is oblique to magmatic differentiation trends observed in the products of earlier Rabaul eruptions and indicates mixing of dacites with a highly magnesian basalt, possibly having 8-10 wt% MgO.

3. The moderately large volume SO_2 flux observed in the Tavurvur emission plume (and the absence of SO_2 in the Vulcan plume) combined with high dissolved S contents (~1800 ppm) in basaltic melt inclusions trapped in olivine of Tavurvur eruptives indicates that the injected basaltic magma was confined to the eastern to northeastern sector (Tavurvur-side) of the sub-caldera dacite reservoir.

4. H_2O and CO_2 volatile contents of dacitic melt inclusions and the caldera-extensive seismic low-velocity zone defined by the 1997 RELACS seismic tomography experiment are consistent with the presence of an extensive dacitic magma reservoir at a depth of ~3-6 km. The much higher H_2O and CO_2 contents of basaltic melt inclusions reflect the crystallisation of the basalt at depths of ~5 to 9 km prior to interaction with the dacite.

5. Mass balance calculations based on the S contents of basaltic melt inclusions (i.e. 1800 ppm) and the moderately large SO_2 yield from Tavurvur during Phase 1 (i.e. 500 ktons, based on TOMS and COSPEC data from Roggensack et al. 1996) provide the basis for an estimate of

~0.1 km^3 for the volume of injected and degassed basaltic magma. This is about 2-3 orders of magnitude smaller than a suggested volume of 15-150 km^3 for the shallow dacite-filled magma reservoir, but sufficient to cause rupture of the reservoir.

6. The 1994 eruptions were likely triggered by and evolved in response to multiple magma injection events that took place over a period of at least 23 years prior to the onset of the eruption. Differences between the dacite magma compositions erupted in 1878, 1937-1943 and 1994-2001, the presence of zoned plagioclase phenocrysts reflecting older basalt-dacite magma interaction events (i.e. anorthite cores overgrown with thick andesine rims) and the occurrence of major intra-caldera seismo-deformational events indicate that the shallow magma system at the Rabaul Caldera Complex is subjected to repeated mafic magma injections at intervals of several years to several decades.

ACKNOWLEDGEMENTS

We thank Shane Nancarrow, formerly of Geoscience Australia, for making many aspects of this project possible and AusAid for providing financial support to HP to undertake research at the Australian National University (ANU) into the 1994 and historical eruptions at Rabaul. The following ANU staff are acknowledged for their support: Bruce Chappell, Ulrich Seniff and John Pike facilitated XRF analyses, Nick Ware and Frank Brink assisted with electronprobe microanalyses, and Michael Shelley, Charlotte Allen and Les Kinsley helped with ICPMS analyses over the duration of this study. We also thank Ima Itikarai, Oli Gudmunsson, and Doug Finlayson for providing advice on the interpretation of seismic data and the RELACS tomographic experiment results, and Hugh Davies of Earth Sciences Division, University of Papua New Guinea (UPNG), for sharing results obtained on 1994-2001 eruption ashes. We gratefully acknowledge reviews of the manuscript provided by: Hugh Davies, Gareth Fabbro of Earth Observatory Singapore, Nanyang Technological University, Singapore, John Pallister, US Geological Survey, and C. Dan Miller, US Geological Survey. COM publishes with the permission of the Secretary, Mr. Harry Kore, Department of Mineral Policy and Geohazards Management, Papua New Guinea.

REFERENCES

Anderson, A.T., 1976. Magma mixing: petrological process and volcanological tool. Journal of Volcanology and Geothermal Research, 1(1), 3-33.

Bai, C. and Greenhalgh, S., 2005. 3-D multi-step travel time tomography: imaging the local, deep velocity structure of Rabaul Volcano, Papua New Guinea. Physics of the Earth and Planetary Interiors, 151, 259-275.

Blake S., 1981. Volcanism and the dynamics of open magma chambers. Nature, 289, 783-785

Blong, R. and McKee, C.O., 1995. The Rabaul eruption: destruction of a town. Natural Hazards Research Centre, Macquarie University.

Bouvet de Maisonneuve, C., Costa, F., Patia, H., and Huber, C., 2015. Mafic magma replenishment, unrest and eruption in a caldera setting: insights from the 2006 eruption of Rabaul (Papua New Guinea). In: Caricchi, L. and Blundy, J.D., (eds) Chemical, Physical and Temporal Evolution of Magmatic Systems. Geological Society, London, Special Publication, 422.

Brown, G., 1878. Journal of the Rev. G. Brown 1860-1902 (11 volumes). Mitchell Library, Sydney, Australia.

Cashman, K.V., Sparks, R.S.J. and Blundy, J.D., 2017. Vertically extensive and unstable magmatic systems: A unified view of igneous processes. Science, 355, 1280.

Clynne, M.A., 1999. A complex magma mixing origin for rocks erupted in 1915, Lassen Peak, California. Journal of Petrology, 40(1), 105-132.

Cooke, R.J.S., 1977. Rabaul Volcanological Observatory and geophysical surveillance of the Rabaul Volcano. Australian Physicist, February 1977, 27-30.

Coombs, M.L. and Gardner, J.E., 2004. Reaction rim growth on olivine in silicic melts: Implications for magma mixing. American Mineralogist, 89 (5-6), 748-758.

Coombs, M.L., Eichelberger, J.C. and Rutherford, M.J., 2000. Magma storage and mixing conditions for the 1953-1974 eruptions of Southwest Trident volcano, Katmai National Park, Alaska. Contributions to Mineralogy and Petrology, 140 (1), 99-118.

Costa, F., Dohmen, R., and Chakraborty, S., 2008. Time scales of magmatic processes from modelling the zoning patterns of crystals. Reviews in Mineralogy and Geochemistry, 69, 545-594.

Druitt, T.H., Costa, F., Deloule, E., Dungan, M. and Scaillet, B., 2012. Decadal to monthly timescales of magma transfer and reservoir growth at a caldera volcano. Nature, 482 (7383), 77-80.

Eggins, S.M., Woodhead, J.D., Kinsley, L.P.J, Mortimer, G.E., Sylvester, P., McCulloch, M.T., Hergt, J.M., and Handler, M.R., 1997. A simple method for the precise determination of >40 trace elements in geological samples by ICPMS using enriched isotope internal standardisation. Chemical Geology, 134(4), 311-326.

Eggins S.M., 2003. Laser ablation ICPMS analysis of geological materials prepared as Li-borate glasses. Journal of Geostandards and Geoanalysis, 27(2), 147-162. .

Eichelberger, J.C., 1980. Vesiculation of mafic magma during replenishment of silicic magma reservoirs. Nature, 288, 446-450.

Finlayson, D.M., Gudmundsson, O., Itikarai, I., Nishimura, Y., and Shimamura, H., 2003. Rabaul Volcano, Papua New Guinea: seismic tomographic imaging of an active caldera Journal of Volcanology and Geothermal Research, 124: 153-171.

Fisher, N.H., 1939. Geology and Vulcanology of Blanche Bay, and Surrounding Area, New Britain. Territory of New Guinea Geological Bulletin, 1, 68pp.

Gardner, J.E., Carey, S., Rutherford, M.J. and Sigurdsson, H., 1995. Petrologic diversity in Mount St. Helens dacites during the last 4,000 years: implications for magma mixing. Contributions to Mineralogy and Petrology, 119: 224-238.

Gerlach, D.C. and Grove, T.L., 1982. Petrology of Medicine Lake Highland Volcanics: Characterization of Endmembers of Magma Mixing. Contributions to Mineralogy and Petrology, 80, 147-159.

Gill, J.B., 1981. Orogenic Andesites and Plate Tectonics. Springer-Verlag, Berlin, 390 pp.

GVN, 1994. Rabaul. Bulletin of the Global Volcanism Network, 19(8), 2-6, and 19(9), 4-7.

Hawkesworth, J., Byron, J., Wallis, S., Carteret, P., Cook, J. and Banks, J., 1773. An account of the voyages undertaken by the order of His present Majesty for making discoveries in the Southern Hemisphere, and successively performed by Commodore Byron, Captain Wallis, Captain Carteret, and Captain Cook, in the *Dolphin*, the *Swallow* and the *Endeavour*: drawn up from the journals which were kept by the several commanders, and from papers of Joseph Banks esq.; London Printed for W. Strahan and T. Cadell.

Heming, R.F., 1974. Geology and petrology of Rabaul Caldera, Papua New Guinea. Geol. Soc. Am. Bull., 85: 1253-64.

Heming, R.F., 1977. Mineralogy and proposed P-T paths of basaltic lavas from Rabaul Caldera, Papua New Guinea. Contrib. Mineral. Petrol., 61, 15-33.

Heming, R.F., and Carmichael I.S.E., 1973. High temperature pumice flows from Rabaul Caldera, Papua New Guinea. Contrib. Mineral. Petrol., 38, 1-20.

Herrmann W., and Berry, R.F., 2002. MINSQ – a least squares spreadsheet method for calculating mineral proportions from whole rock major element analyses. Geochemistry: Exploration, Environment, Analysis. 2, 361-368.

Huppert, H,E., Sparks, R.S. J. and Turner, J.S., 1982. Effects of volatiles on mixing in calc-alkaline magma systems. Nature, 297, 554-557.

Itikarai, I., 2008. The 3-D structure and earthquake locations at Rabaul Caldera, Papua New Guinea. M. Phil. Thesis, The Australian National University, Canberra.

Izbekov, P.E., Eichelberger, J.C. and Ivanov, B.V., 2004. The 1996 Eruption of Karymsky Volcano, Kamchatka: Historical Record of Basaltic Replenishment of an Andesite Reservoir. Journal of Petrology, 45 (11), 2325-2345.

Izbekov, P.E., Eichelberger, J.C., Patino, L.C., Vogel, T.A. and Ivanov, B.V., 2002. Calcic cores of plagioclase phenocrysts in andesite from Karymsky volcano: Evidence for rapid introduction by basaltic replenishment. Geology, 30 (9), 799-802.

Johnson, R.W., and Threlfall, N.A., 1985. Volcano Town - the 1937-43 Eruptions at Rabaul, Robert Brown and Associates, Bathurst, Australia, 151 pages.

Johnson, R.W., Everingham, I.B., and Cooke, R.J.S., 1981. Submarine volcanic eruptions in Papua New Guinea: 1878 activity of Vulcan (Rabaul) and other examples. In: Johnson, R.W., (ed) Cooke-Ravian Volume of Volcanological Papers. Geological Survey of Papua New Guinea Memoir 10: 167-179.

Johnson, R.W., McKee, C.O., Eggins, S., Woodhead, J., Arculus, R.J., Chappell, W. and Sheraton, J., 1995. The 1994 eruptions at Rabaul Volcano, Papua New Guinea: taking petrologic pathways towards understanding a restless caldera. EOS, Transactions of the American Geophysical Union, 76: 171.

Johnson, R.W., Itikarai, I., Patia, H. and McKee, C.O., 2010. Volcanic systems of the Northeastern Gazelle Peninsula, Papua New Guinea: synopsis, evaluation, and a model for Rabaul Vocano. Rabaul Volcano Workshop Report, Papua New Guinea Department of Mineral Policy and Geohazards Management, and Australian Agency for International Development, Port Moresby, 84 pages.

Jones, R.H., and Stewart R.C. 1997. A method for determining significant structures in a cloud of earthquakes. Journal of Geophysical Research, 94, 8245-8254.

Kent, A.J.R., Darr, C., Koleszar, A.M., Salisbury, M.J. and Cooper, K.M., 2010. Preferential eruption of andesitic magmas through recharge filtering. Nature Geoscience, 3, 631-636.

Lindsley, D.H., 1983. Pyroxene thermometry. American Mineralogist, 68, 477-493.

McKee, C.O., 2015. Tavui Volcano: neighbour of Rabaul and probable source of the penultimate major eruption in the Rabaul area. Bulletin of Volcanology, 77: 80.

McKee, C.O. and Duncan, R.A., 2016. Early volcanic history of the Rabaul area. Bulletin of Volcanology, 78: 24.

McKee, C.O, Mori, J. and Talai, B., 1989. Microgravity changes and ground deformation at Rabaul Caldera, 1973-1985. In: J.H. Latter (Ed.) Volcanic Hazards Assessment and Monitoring, Springer-Verlag, 399-428.

McKee, C.O., Neall, V.E. and Torrence, R., 2011. A remarkable pulse of large-scale volcanism on New Britain Island, Papua New Guinea. Bulletin of Volcanology, 73, 27-37.

McKee, C.O., Baillie, M.G. and Reimer, P.J., 2015. A revised age of AD 667-699 for the latest major eruption at Rabaul. Bulletin of Volcanology, 77: 65.

McKee, C.O., Kuduon, J. and Patia, H., 2016. Recent eruption history at Rabaul: volcanism since the 7th century AD caldera-forming eruption. Geohazards Management Division Report 2016/01.

McKee, C.O., Itikarai, I. and Davies, H.L., 2017. Instrumental volcano surveillance and community awareness in the lead-up to the 1994 eruptions at Rabaul, Papua New Guinea. In: Fearnley C. et al., (Eds.), Advances in Volcanology, Observing the Volcano World - Volcano Crisis Communication. Springer, Berlin, 350 p.

McKee, C.O., Lowenstein, P.L., de Saint Ours, P., Talai, B., Itikarai, I and Mori, J, 1984. Seismic and ground deformation crises at Rabaul caldera: Prelude to an eruption? Bulletin of Volcanology, 47, 397-411.

McKee, C.O., Johnson, R.W., Lowenstein, P.L., Riley, S.J., Blong, R.J., de Saint Ours, P. and Talai, B., 1985. Rabaul Caldera, Papua New Guinea: volcanic hazards, surveillance, and eruption contingency planning. Journal of Volcanology and Geothermal Research, 23, 195-237.

McLeod, P. and Tait, C., 1999. The growth of dykes from magma chambers. Journal of Volcanology and Geothermal Research, 92 (3), 231-245.

Mori, J. and McKee, C.O., 1987. Outward-dipping ring fault structure at Rabaul caldera as shown by earthquake locations. Science, 235: 193-195.

Mori, J., McKee, C., Itikarai, I., Lowenstein, P., de Saint Ours, P., Talai, B., 1989. Earthquakes of the Rabaul Seismo-deformation Crisis, September 1983 to July 1985; seismicity on a caldera ring fault: In: J.H. Latter (Ed.) - Volcanic Hazards Assessment and Monitoring, Springer-Verlag, 429-462.

Murphy, M.D., Sparks, R.S., Barclay, J., Carroll, M.R., Lejeune, A.M., Brewer, T.S., MacDonald, R. and Black, S., 1998. The role of magma mixing in triggering the current eruption at the Soufriere Hills Volcano, Montserrat. Geophysical Research Letters, (25), 3433-3436.

Murphy, M.D., Sparks, R.S.J., Barclay, J., Carroll, M.R. and Brewer, T.S., 2000. Remobilization of Andesite Magma by Intrusion of Mafic Magma at the Soufriere Hills Volcano, Montserrat, West Indies. Journal of Petrology, 41 (1), 21-42.

Nairn, I.A., Wood, C.P., Talai, B. and McKee, C.O, 1989. Papua New Guinea – 1:25 000 reconnaissance geological map and eruption history. Report prepared for the Ministry of External Relations and Trade, New Zealand. 75pp.

Nairn, I.A., McKee, C.O., Talai, B. and Wood, C.P., 1995. Geology and eruptive history of Rabaul Caldera, Papua New Guinea. Journal of Volcanology and Geothermal Research, 69: 259-288.

Norrish, K., and Chappell, B.W.C., 1977. X-ray fluorescence spectrometry. In: Zussman, J., (Ed.), Physical Methods in Determinative Mineralogy, 2nd Ed., Academic Press, London, 254-272.

Norrish, K., and Hutton, J.T., 1969. An accurate spectrographic method for analysis of a wide range of geological samples. Geochimica et Cosmochimica Acta, 33, 431-453.

Pallister, J.S., Hoblitt, R.P., Meeker, G.P., Knight, R.J. and Siems, D.F., 1996. Magma mixing at Mount Pinatubo: petrographic and chemical evidence from the 1991 deposits. In: Newhall C.G. and Punongbayan R.S. (Eds), Fire and mud: eruptions and lahars of Mount Pinatubo, Philippines. PHIVOLCS, Quezon City, Philippines and University of Washington Press, 687-731.

Patia. H., 2003. Petrology and Geochemistry of the Recent Eruption History at Rabaul Caldera, Papua New Guinea: implications for magmatic processes and recurring volcanic activity. Master of Philosophy thesis, Australian National University, Canberra.

Patia, H., Eggins, S., McKee, C.O., and Johnson, R.W., 1997. The 1994 to present eruption at Rabaul, Papua New Guinea: evidence of repeated basaltic magma influx into a sub-caldera dacite magma reservoir. Annual meeting of the Volcanological Society of Japan, Abstract.

Roggensack, K., Williams, S.N., Schaefer, S.J., and Parnell, R.A., 1996. Volatiles from the 1994 eruptions of Rabaul: understanding large caldera systems. Science, 273, 490-493.

Saunders S.J., 2001. The shallow plumbing system of Rabaul caldera: a partially intruded ring fault? Bulletin Volcanology, 63, 406-420.

Saunders, S.J., 2006. The possible contribution of circumferential fault intrusion to caldera resurgence. Bulletin of Volcanology, 67, 57-71.

Snyder, D., 2000. Thermal effects of the intrusion of basaltic magma into a more silicic magma chamber and implications for eruption triggering. Earth and Planetary Science Letters, 175, 257-273.

Sparks, S.R.J., Sigurdsson, H. and Wilson, L., 1977. Magma mixing: a mechanism for triggering acid explosive eruptions. Nature, 267(5609), 315-318.

Streck, M.J., 2008. Mineral textures and zoning as evidence for open system processes. Reviews in Mineralogy and Geochemistry, 69(1), 595-622.

Tait, C., Jaupart, C. and Vergniolle, S., 1989. Pressure, gas content and eruption periodicity of shallow water crystallising magma chambers. Earth Planetary Science Letters, 92: 107-123.

Tepley III. F.J., Davidson, J.P., Tilling, R.I. and Arth, J.G., 2000. Magma mixing, recharge and eruption histories recorded in plagioclase phenocrysts from El Chichon Volcano, Mexico. Journal of Petrology, 41 (9), 1397-1411.

Thomas, N. and Tait, S.R., 1997. The dimensions of magmatic inclusions as a constraint on the physical mechanism of mixing. Journal of Volcanology and Geothermal Research, 75, 167-178.

Walker, G.P.L., Heming, R.F., Sprod, T.J. and Walker, H.R., 1981. Latest major eruptions of Rabaul Volcano. In: R.W. Johnson (Ed.) Cooke-Ravian Volume of Volcanological Papers, Geological Survey of Papua New Guinea. Memoir 10: 181-193.

Wallace, D.A. and Tufar, W., 1998. OLGA II oceanographic survey of Tavui Caldera, Rabaul. Australian Geological Survey Organisation, Canberra.

Wallace, P., Eggins, S. and Arculus, R., 2002. Pre-1400 BP magmatic history of Rabaul, PNG. Abstracts of the 16th Australian Geological Convention (Adelaide), 67: 253.

Wallis, H. (Editor), 1965. Carteret's Voyage Round the World, 1766-1769. Hakluyt Society, Cambridge.

White, R.A., 1996. Precursory deep long-period earthquakes at Mount Pinatubo, Philippines: Spatio-temporal link to a basalt trigger. In: Newhall C.G. and Punongbayan R.S. (Eds), Fire and mud: Eruptions and lahars of Mount Pinatubo, Philippines. PHIVOLCS, Quezon City, Philippines and University of Washington Press, 687-731.

Wood, C.P., Nairn, I.A., McKee, C.O., and Talai, B., 1995. Petrology of Rabaul Caldera, Papua New Guinea. Journal of Volcanology and Geothermal Research, 69: 285-302.

FIGURES

1. Rabaul Caldera Complex showing Vulcan and Tavurvur, the active vents during the 1994 eruptions, and other intra-caldera vents (solid triangles), the nested caldera structure (bold curved lines), the zone of caldera seismicity (stippled), the NW to SE alignment (the W-T Zone) of stratovolcanoes Watom, Tovanumbatir, Kabiu, Palangiangia, and Turagunan (open triangles), and Tavui Caldera to the north. Rabaul Town occupies the N part of the caldera complex.

2. Transmitted light photomicrographs (XPL) illustrating characteristic morphologies and associations of phenocrysts in Vulcan and Tavurvur dacites and andesites erupted during the 1994-2001 period. Plate A shows a phenocryst aggregate comprising euhedral plagioclase (andesine) with abundant melt inclusions (denoted MI), clinopyroxene (cpx), orthopyroxene (opx) and titano-magnetite (Ti-mag), interstitial glass and surrounding microcrystalline groundmass (gmass) with vesicles (field of view = 3x2 mm). Plate B shows a large euhedral olivine phenocryst (Fo_{84}), and several plagioclase and clinopyroxene microphenocrysts from a Tavurvur andesite (field of view = 3x2 mm). Plate C shows a small euhedral plagioclase phenocryst of labradorite composition enclosing several apatite rods (field of view = 1.5x1 mm). Plate D shows part of a large plagioclase phenocryst comprising a mottled anorthitic (An_{93}) core containing many large melt inclusions, that is overgrown by a thin, melt inclusion-free labradorite rim that also bears several apatite needles (field of view = 1.5x1 mm).

3. Plagioclase sub-ternary plots showing the large range of plagioclase phenocryst compositions analysed from the 1994-2001 eruptives. Note the virtually identical and very large range of compositions (andesine through to anorthite) occurring in both Vulcan and Tavurvur eruptives, and in both the Phase 1 and Phase 2 products of Tavurvur.

4. Pyroxene and olivine phenocryst compositions from 1994-2001 eruptives plotted on the magnesian side (Mg/(Mg+Fe) >0.50) of the pyroxene quadrilateral. Note the more limited

range and more Fe-rich compositions of clinopyroxene in the Vulcan eruptives, and also the similar fields of clinopyroxene compositions that range to considerably more Mg-rich clinopyroxene compositions in both the Phase 1 and Phase 2 products of Tavurvur. Note also the range of orthopyroxene compositions, and the olivine compositions plotted along the baseline. Tie-lines link coexisting clinopyroxene-orthopyroxene pairs, and isotherms are taken from the graphical pyroxene thermometer of Lindsley (1983).

5. Histograms showing the range and frequency distribution of plagioclase and clinopyroxene phenocryst compositions in the 1994-2001 eruptives. Note the strongly bimodal distribution of clinopyroxene compositions. Also note the dominance of the andesine-labradorite plagioclase phenocrysts, and the development of secondary modes at more calcic compositions, particularly in the highly calcic range An_{86-96}.

6. Core and rim compositions analysed in plagioclase phenocrysts from 1994-2001 eruptives of Vulcan and Tavurvur. Note the clustering of phenocrysts near the 1:1 line (i.e. similar core and rim compositions) with compositions in the ranges An_{50-60} and An_{86-96}, and the large number of phenocrysts that have An_{50-60} compsitions but also have anorthite-rich cores ('old' cores). Further note that no Vulcan phenocrysts are represented in the cluster with An_{86-96} cores and rims.

7. Comparison of K_2O versus SiO_2 whole rock compositions of 1994-2001 eruptives to a compilation of compositions from previous Rabaul eruptions (data compiled from Heming 1974; Wood et al., 1995; this study; and our unpublished data). Shown for reference are basalt-basaltic andesite-andesite-dacite-rhyodacite-rhyolite and the low-, medium- and high-K discriminant fields (after Gill, 1981). Note the tight linear trend of the 1994-2001 compositions, which range from andesite through to dacite. A group of Raluan Ignimbrite rhyolite analyses is geochemically distinct from all other analyses. The Raluan compositions have been shown to be inconsistent with derivation by crystal fractionation of observed

crystalline phases from Rabaul rhyodacites and dacites (Wood et al., 1995). The Raluan Ignimbrite may have originated from the neighbouring Tavui system (Wallace et al., 2002; McKee, 2015).

8. Major element vs MgO variation diagrams comparing the whole-rock compositions (calculated on a volatile-free basis) for 1994-2001 eruptives of Vulcan and Tavurvur with the compositions of previous eruptives. Earlier eruptives are divided into pre-1400 BP and post-1400 BP groups, with additional distinction made of the 1878 and 1937-43 eruptives from Vulcan and Tavurvur, and analyses from the Raluan Ignimbrite and 1400 BP Rabaul Pyroclastics. The large arrows show the linear mixing trends formed by 1994-2001 eruptives, which begin at dacite compositions and extend through andesites toward a mafic basalt composition. Note the oblique nature of these trends relative to other Rabaul magma compositions.

9. Trace element vs MgO variation diagrams comparing the whole-rock compositions of 1994-2001 eruptives of Vulcan and Tavurvur with the compositions of previous eruptives. Earlier eruptives are divided into pre-1400 BP and post-1400 BP groups, with additional distinction made of the 1878 and 1937-43 eruptives from Vulcan and Tavurvur, and the 6900 BP Raluan Ignimbrite and the 1400 BP Rabaul Pyroclastics. The large arrows show the linear mixing trends formed by 1994-2001 eruptives, which begin at dacite compositions and extend through andesites toward a mafic basalt composition. Again note the oblique nature of these trends relative to other Rabaul magma compositions.

10. Temporal evolution of the MgO whole-rock compositions of erupted products through the course of the 1994-2001 eruptive period. Vertical lines show the timing of strombolian eruptions during Tavurvur's Phase 2 activity, and arrows show trends in the maximum MgO compositions of andesites and in the minimum MgO compositions of dacites. Compositions of 1878 and the 1937-43 eruptives are shown for reference.

11. Schematic representation of a general model for the Rabaul-region magma systems. View is a projection onto a plane orthogonal to the WTZ magma system which occupies a NW-trending tabular zone, shown here bounded by vertical dashed straight lines, separating the Rabaul and Tavui systems. Mantle-derived basaltic magmas ascend to, accumulate and underplate at the crust/mantle boundary. Subsequently magma ascends from the crust/mantle boundary to mid-crustal reservoirs beneath the caldera systems and differentiates to more-evolved compositions. Evolved magmas ascend from mid-crustal reservoirs and feed the sub-caldera magma reservoirs of the Rabaul and Tavui systems. The sub-caldera magma reservoirs for the Rabaul and Tavui systems are shown at different depths, and that for Tavui is shown with a dashed-line boundary reflecting the results of geophysical imaging and the possibility that the Tavui sub-caldera magma reservoir is ephemeral. The active caldera ring fault at Rabaul is shown by the outward-dipping dashed lines. Basaltic magmas from the WTZ intersect the NE edge of the Rabaul sub-caldera magma system, mix with felsic magma and may trigger eruptions at Rabaul. Less-felsic magmas rising from mid-crustal reservoirs also may destabilize the sub-caldera systems resulting in eruptions.

TABLES

1. Rabaul Volcano eruption history, 1400 BP to present – adapted from McKee et al. (2016) and Nairn et al. (1995).
2. Whole-rock major and trace element data for representative samples of Tavurvur and Vulcan products, 1994-2001.
3. Least squares mixing model results.

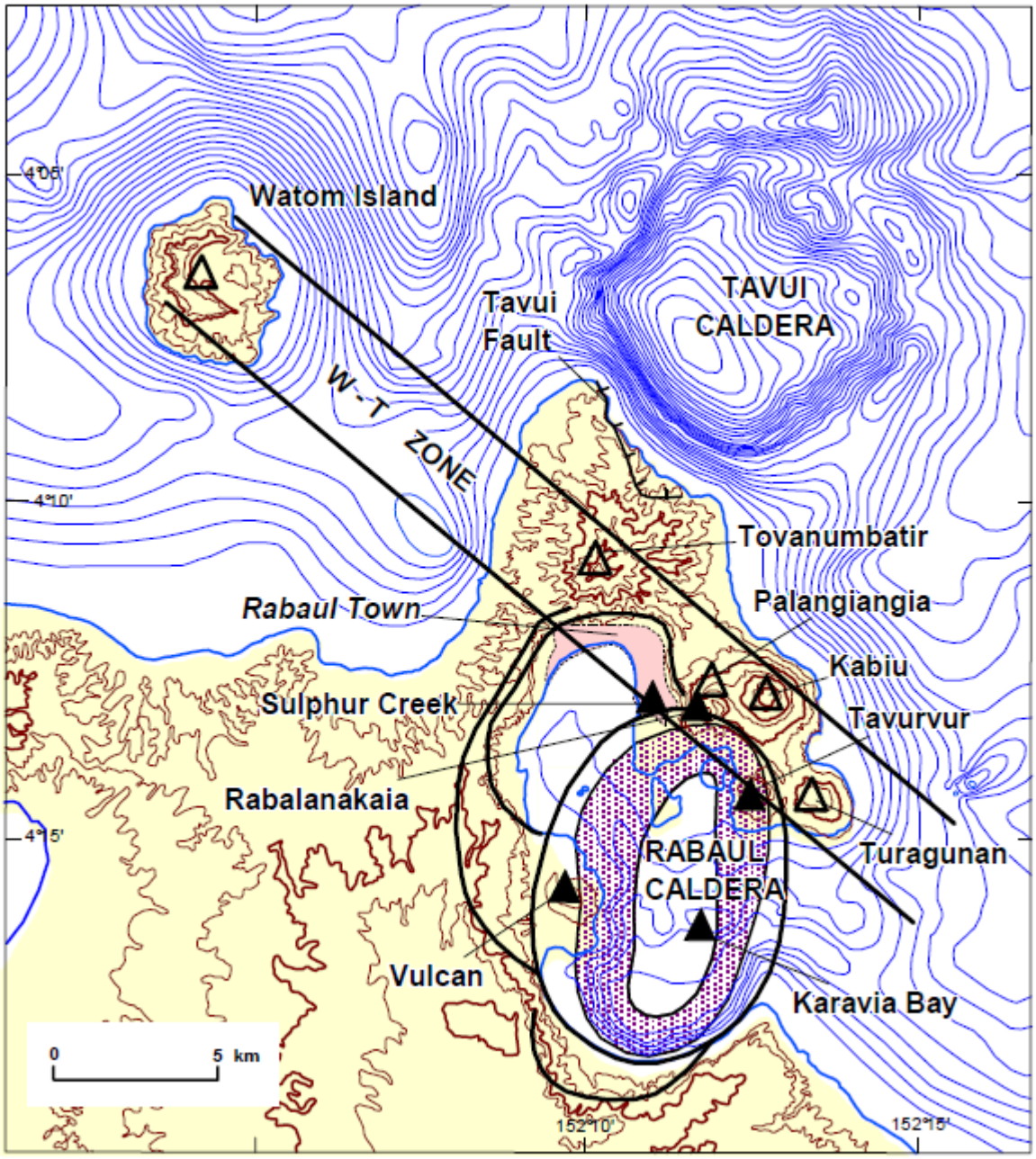

Figure 1

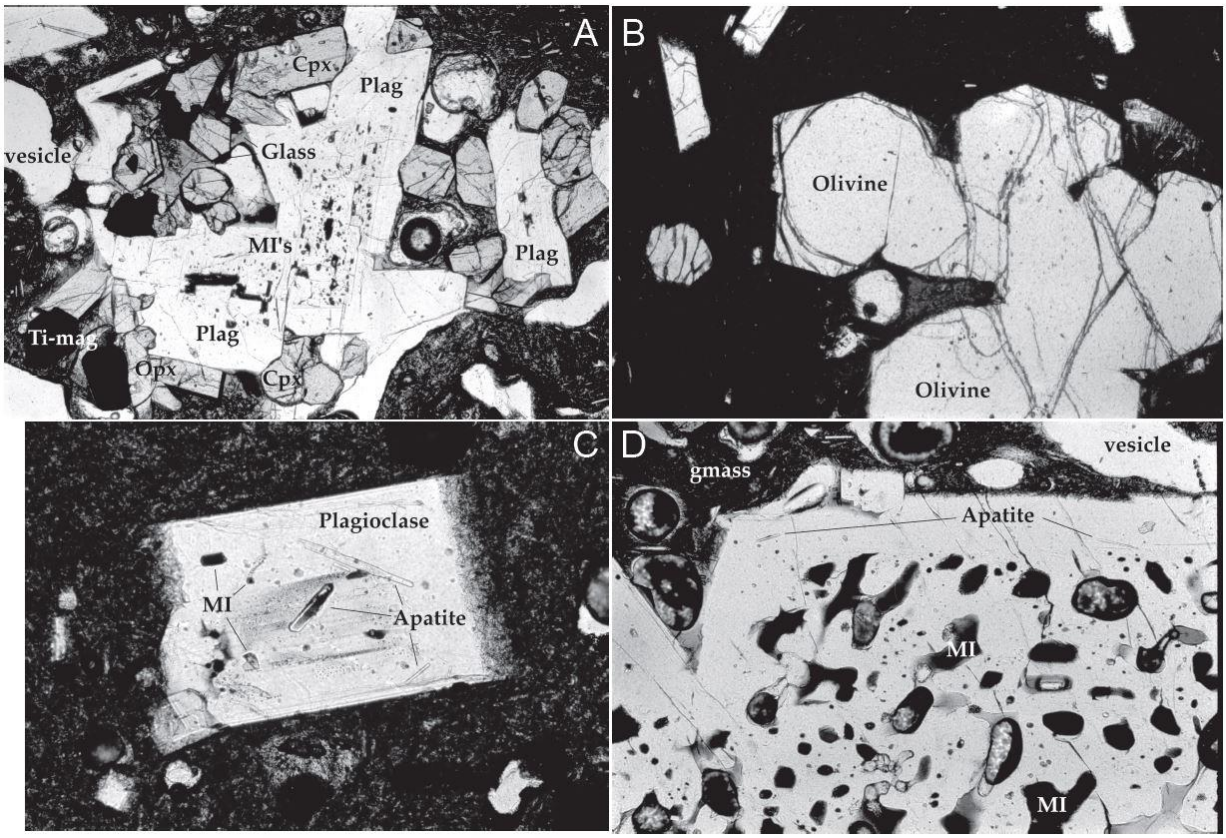

Figure 2

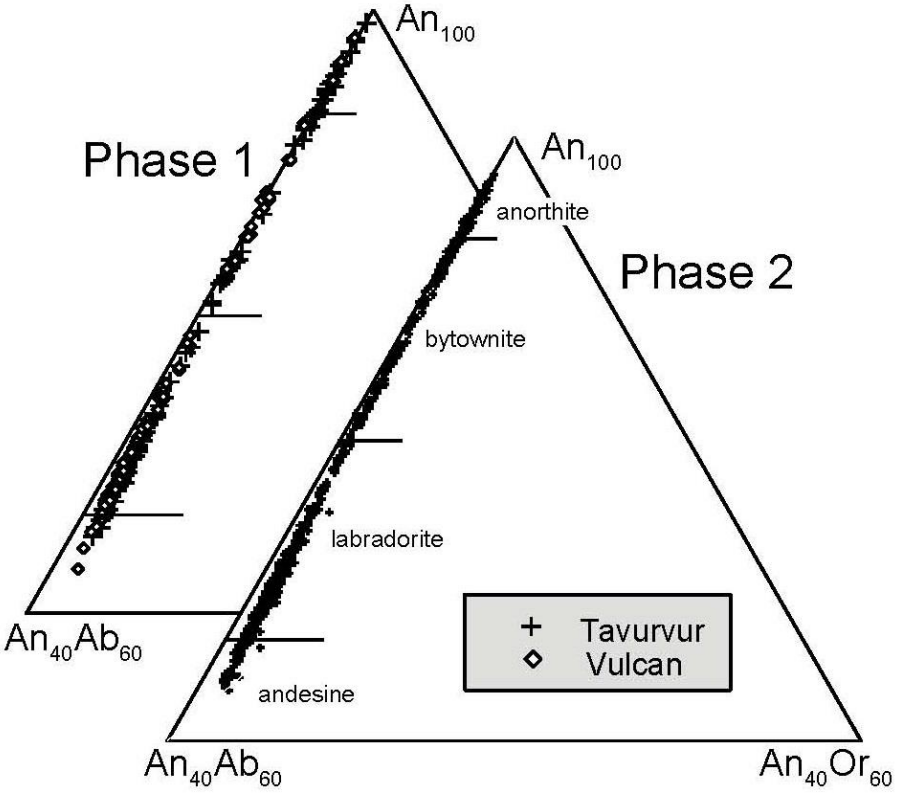

Figure 3

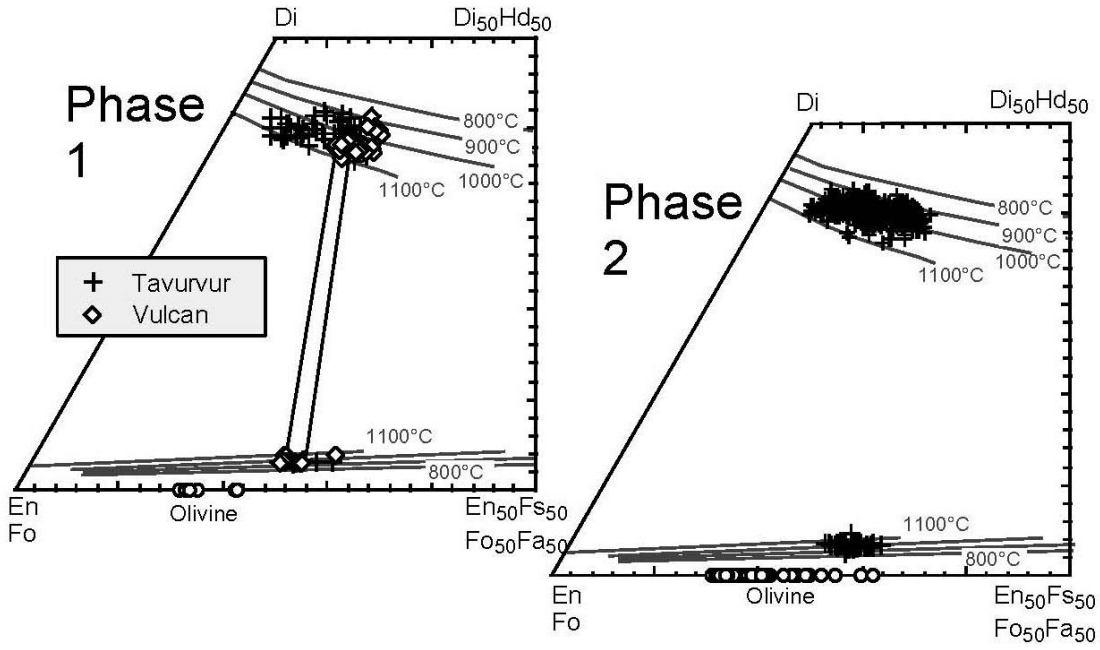

Figure 4

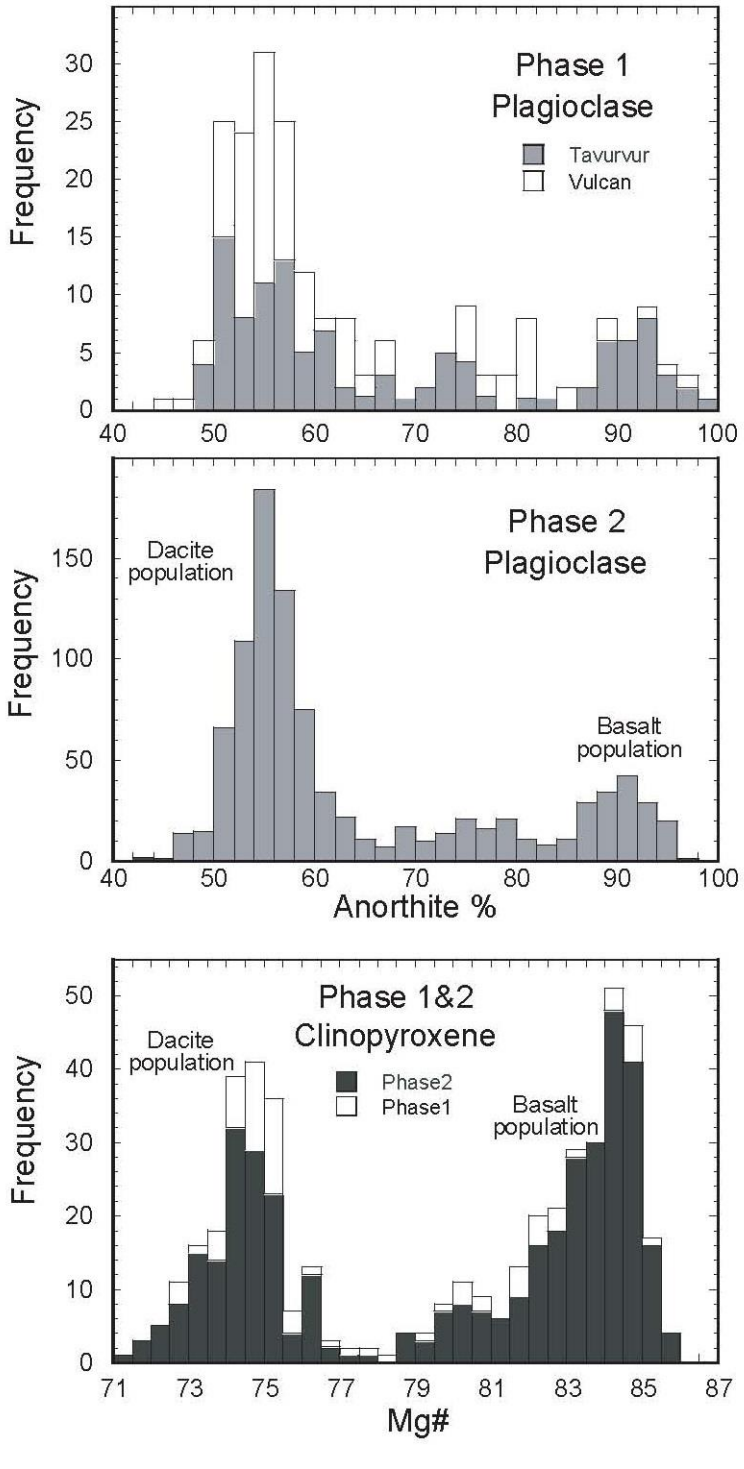

Figure 5

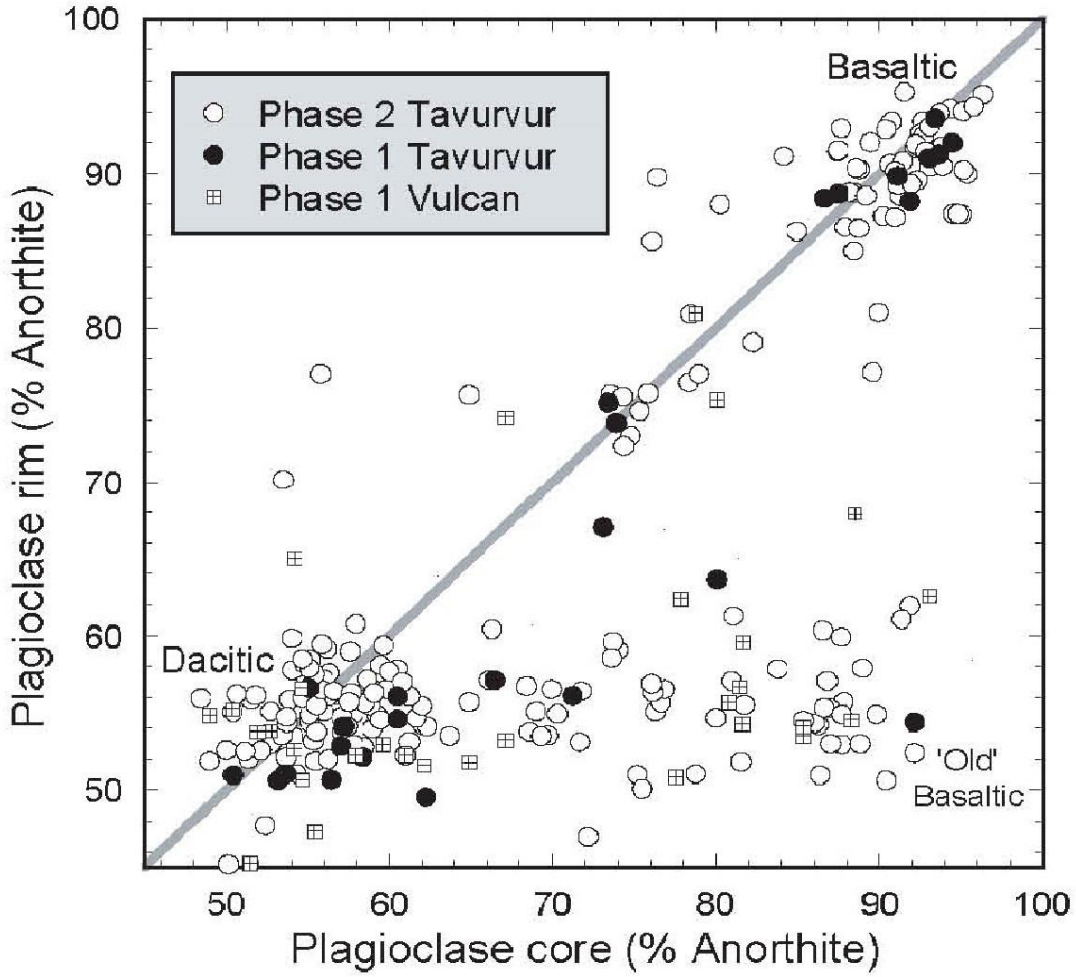

Figure 6

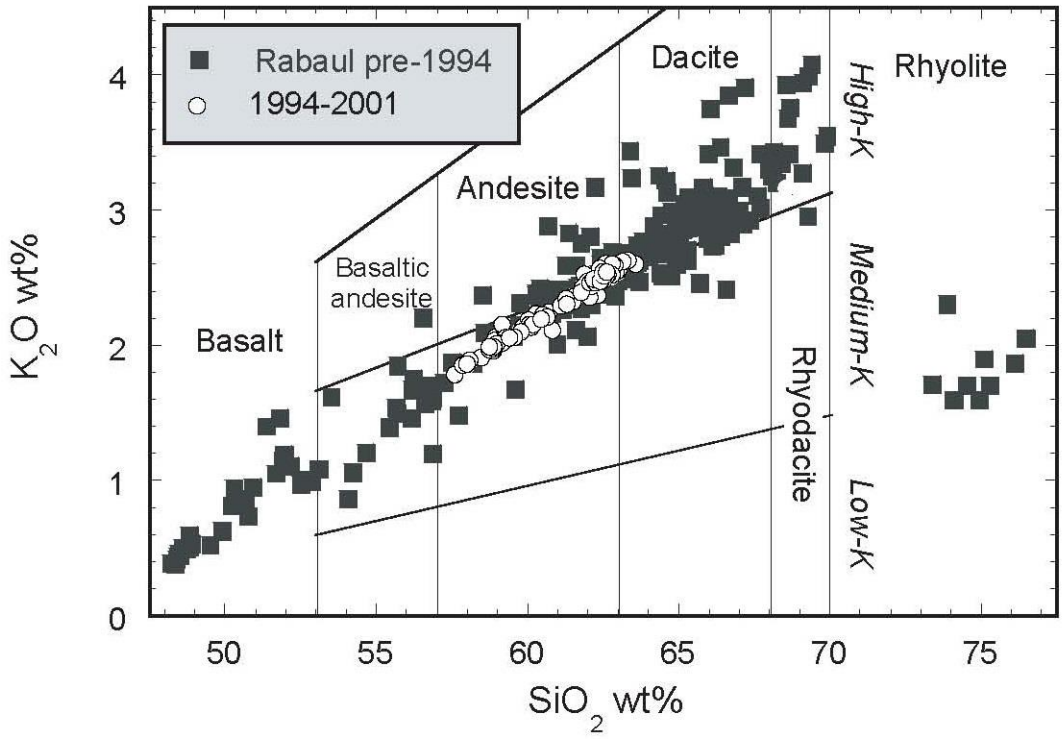

Figure 7

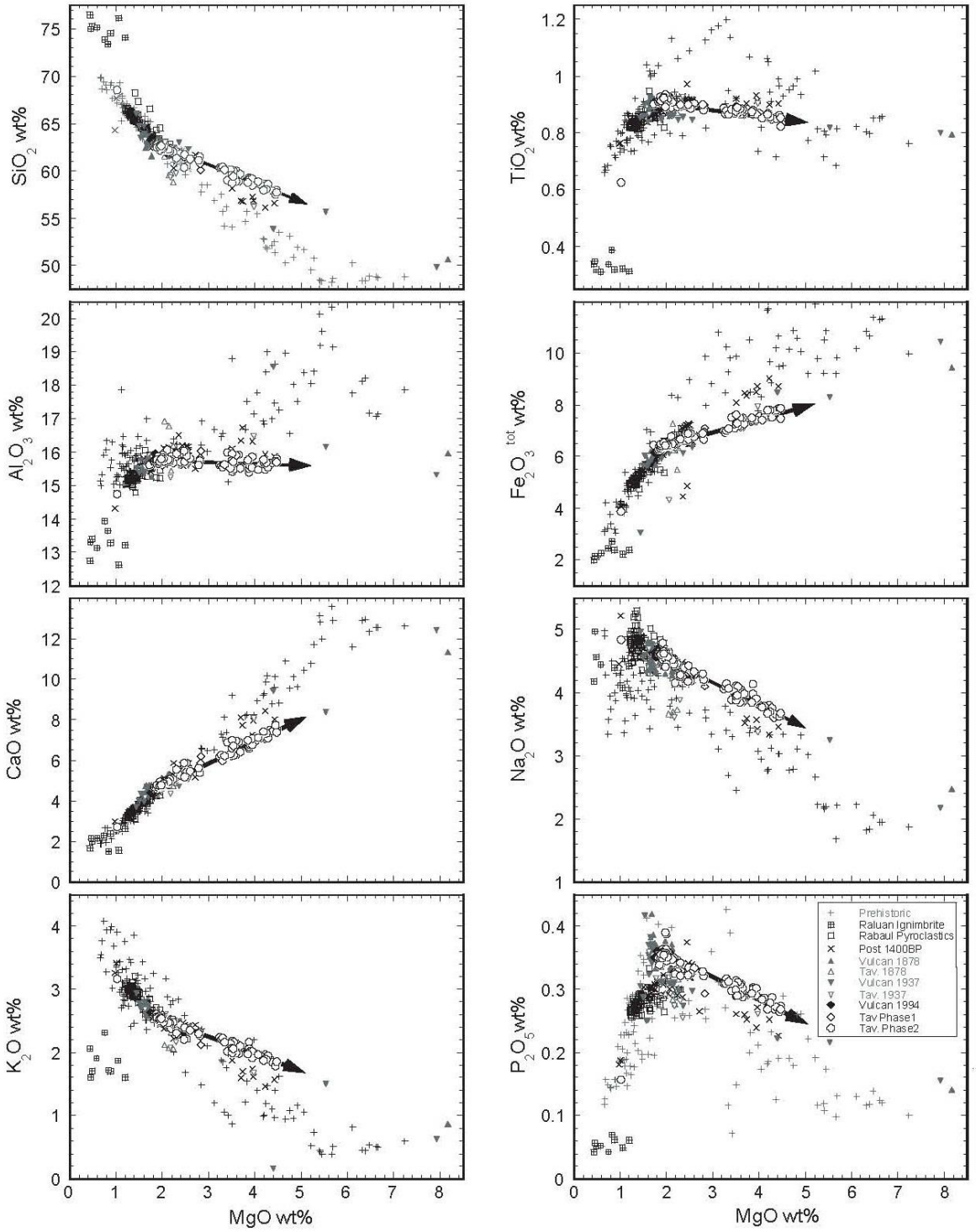

Figure 8

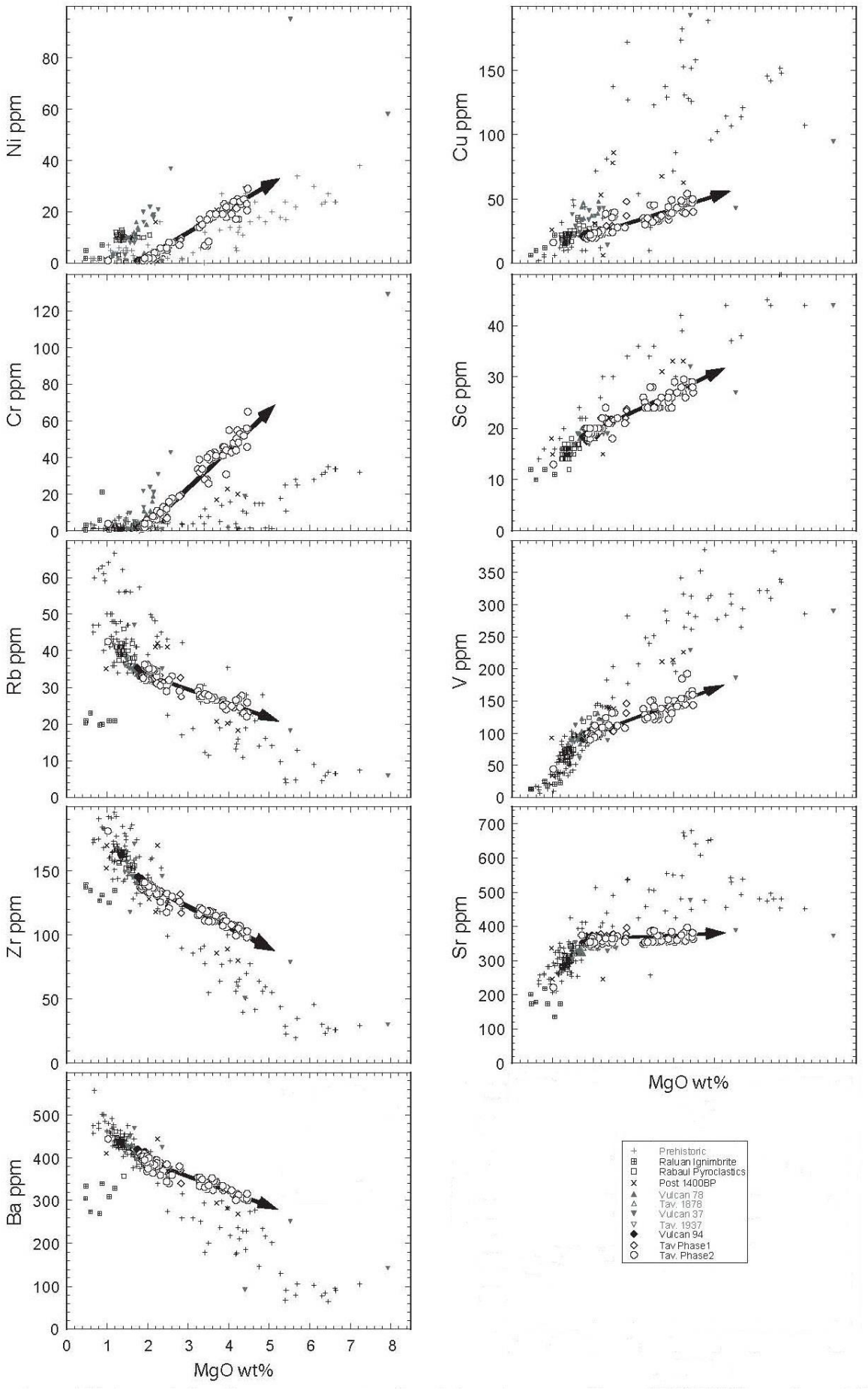

Figure 9

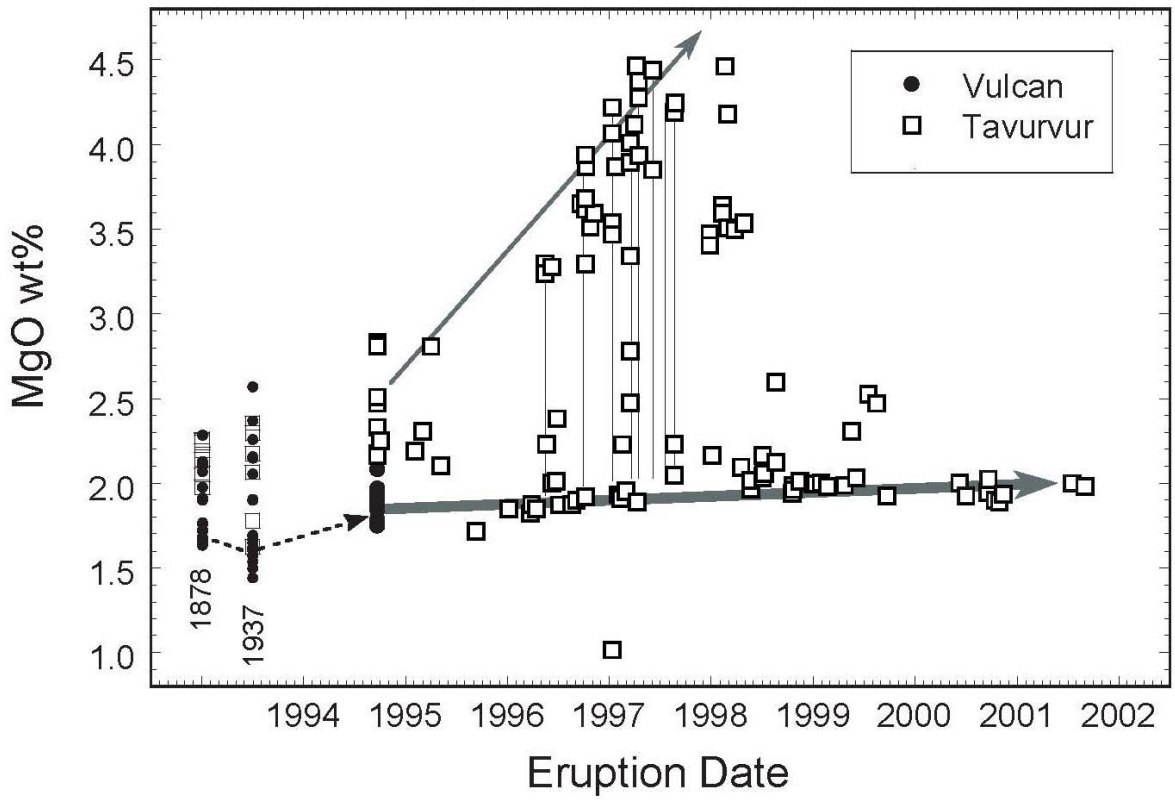

Figure 10

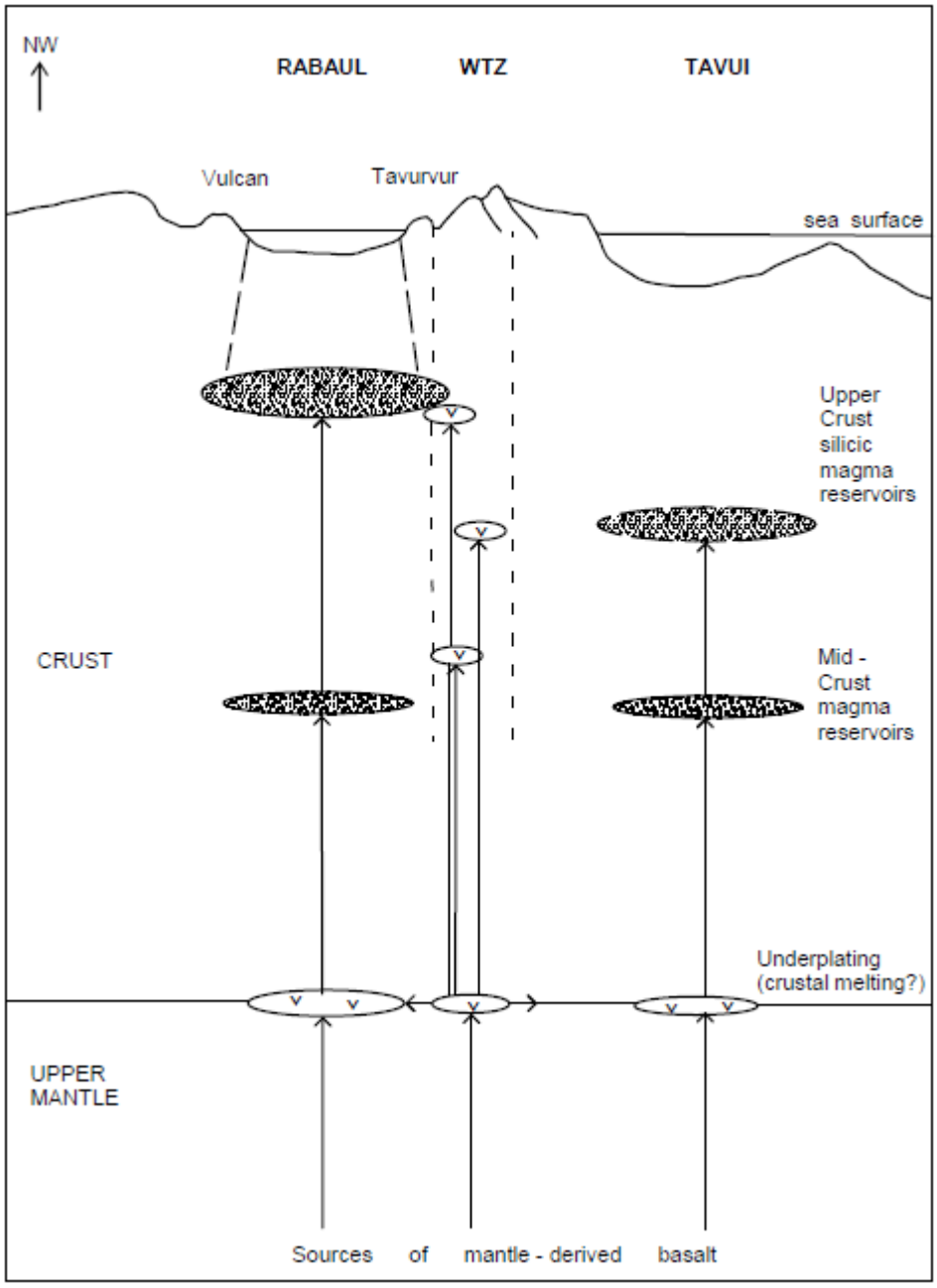

Figure 11

TABLE 1. RABAUL CALDERA - ERUPTION HISTORY 1400 BP TO PRESENT, ADAPTED FROM MCKEE ET AL. (2016) AND NAIRN ET AL. (1995)

AGE	SOURCE, EVENT	VOLUME (KM^3)
A.D. 1994-2014 ...	TAVURVUR PYROCLASTIC & LAVA ERUPTIONS	0.3
1994	VULCAN PYROCLASTIC & CONE-BUILDING ERUPTION	0.3
1937-1943	TAVURVUR PYROCLASTIC ERUPTIONS	0.005
1937	VULCAN PYROCLASTIC & CONE-BUILDING ERUPTION	0.3
1878	TAVURVUR PYROCLASTIC ERUPTION	0.05
1878	VULCAN SUBMARINE, PYROCLASTIC CONE-BUILDING ERUPTION	0.3
CA. 1850	SULPHUR CREEK PYROCLASTIC, CRATER-FORMING ERUPTIONS	?
0.01		
1791	TAVURVUR PYROCLASTIC (& LAVA?) ERUPTION	?
1767	RABALANAKAIA? PYROCLASTIC (& LAVA?) ERUPTION	?
YEARS BP (^{14}C)		
175	RABALANAKAIA PYROCLASTIC ERUPTION → PYROCLASTIC FLOWS	
?		
200	TAVURVUR PROLONGED PYROCLASTIC (& LAVA?) ERUPTIONS	0.1?
?	VULCAN SUBMARINE PYROCLASTIC ERUPTION	?
235	RABALANAKAIA PYROCLASTIC ERUPTION	?
250	RABALANAKAIA LAVA AND PYROCLASTIC ERUPTIONS	?
270	TAVURVUR PYROCLASTIC ERUPTION	?
?	SULPHUR CREEK, PYROCLASTIC (AND LAVA?) CONE-BUILDING ERUPTIONS	?
?	RABALANAKAIA PYROCLASTIC (AND LAVA?) CONE-BUILDING ERUPTIONS	?
?	TAVURVUR PYROCLASTIC (AND LAVA?) CONE-BUILDING ERUPTIONS	?
?	KARAVIA BAY, SUBMARINE PYROCLASTIC CONE-BUILDING ERUPTIONS	0.3?
PRE-770	GREET HARBOUR? SUBMARINE, PYROCLASTIC CONE-BUILDING ERUPTION - PUMICE RAFTS LED TO FORMATION OF MATUPIT PUMICE SEDIMENTS	1.0?
1400	RABAUL PYROCLASTICS ERUPTION AND CALDERA FORMATION	>10

Table 2. Whole-rock major and trace element geochemical data

Sample#	TAVQ-817		TAVT820	TAVW-823	VULA-801		VULM-813	VULP-816	VULN-814	VULG-807
Date	19-Sep-94		19-Sep-94	19-Sep-94	19-Sep-94		19-Sep-94	19-Sep-94	19-Sep-94	19-Sep-94
SiO2	59.46		61.57	62.58	63.21		63.37	61.66	63.48	63.40
TiO2	0.880		0.890	0.904	0.912		0.912	0.895	0.912	0.904
Al2O3	15.88		15.91	15.81	15.79		15.82	15.64	15.81	15.79
Fe2O3	7.02		6.67	6.47	6.40		6.46	6.24	6.35	6.19
MnO	0.155		0.164	0.160	0.160		0.160	0.160	0.160	0.160
MgO	2.81		2.48	2.18	1.92		1.97	1.84	1.86	1.80
CaO	6.13		5.52	5.06	4.68		4.76	4.55	4.69	4.44
Na2O	4.06		4.32	4.43	4.68		4.64	4.66	4.58	4.61
K2O	2.10		2.36	2.48	2.55		2.53	2.57	2.58	2.63
P2O5	0.290		0.330	0.329	0.363		0.363	0.352	0.363	0.352
S wt	0.240		0.012	<0.005	<0.005		0.020	<0.005	<0.005	0.030
Total	99.03		100.23	100.39	100.66		101.00	98.57	100.79	100.31
Ppm	SN-ICPMS	LA-ICPMS	SN-ICPMS	SN-ICPMS	SN-ICPMS	LA-ICPMS	SN-ICPMS	SN-ICPMS	SN-ICPMS	SN-ICPMS
Sc XRF	23.8		20.9	19.3	18.9		19.1	18.5	18.5	18.4
V XRF	146		104	103	102		99	89	89	92
Cr XRF	20		12	9	3		3	2	3	2
Ni XRF	10		6	4	<1		<1	<1	<1	<1
Cu XRF	48		29	26	22		23	22	23	20
Zn XRF	96		90	92	95		93	95	92	94
Ga XRF	16.5		17.0	17.0	16.5		17.0	17.0	17.5	17.0
Rb	28.8	27.7	30.1	31.6	34.5	32.8	32.3	33.1	35.8	36.1
Rb XRF	27.5		31.5	32.5	33.5		34.0	34.0	34.5	35.0
Sr	390	395	365	359	348	364	366	349	347	357
Sr XRF	395		376	367	364		366	362	371	356
Y	34.0	34.0	36.2	36.9	39.5	38.2	38.4	39.7	40.1	40.5
Y XRF	30.0		33.0	34.0	35.0		34.0	35.0	35.0	36.0
Zr	120.2	124.3	135.0	142.3	148.2	143.9	145.3	151.1	152.2	151.4
Zr XRF	117.0		131.0	136.0	141.0		141.0	144.0	144.0	146.0
Nb	2.58	2.57	2.87	3.01	3.18	3.07	3.11	3.20	3.24	3.24
Nb XRF	2.0		2.0	2.0	2.0		2.0	2.0	2.0	2.0
Cs	0.828		0.877	0.922	0.986		0.951	0.997	0.957	0.982
Ba	348	345	388	407	419	406	410	425	404	434
Ba XRF	340		375	395	410		415	400	400	420
La	11.68	11.98	12.40	12.89	13.74	13.93	13.14	13.78	14.28	14.43
Ce	26.20	26.49	28.75	30.12	31.57	30.87	30.70	31.52	32.17	32.19
Ce XRF	30		32	34	32		36	34	32	36
Pr	3.94	3.86	4.23	4.40	4.62	4.54	4.54	4.72	4.74	4.75
Nd	18.04	18.02	19.41	20.43	21.38	21.02	20.80	21.55	21.84	21.68
Sm	4.68	4.93	5.02	5.20	5.44	5.61	5.34	5.48	5.67	5.68
Eu	1.367	1.388	1.444	1.480	1.524	1.554	1.526	1.531	1.583	1.574
Gd	5.10	5.46	5.42	5.67	5.91	6.08	5.82	6.01	6.07	6.02
Tb	0.832		0.891	0.918	0.956		0.951	0.975	0.986	0.975
Dy	5.14	5.65	5.51	5.73	5.97	6.25	5.84	5.99	6.06	6.01
Ho	1.123		1.217	1.249	1.311		1.279	1.317	1.323	1.336
Er	3.32	3.52	3.60	3.74	3.83	4.00	3.80	3.94	3.93	3.95
Yb	3.28	3.60	3.55	3.69	3.88	4.04	3.80	3.90	3.90	3.90
Lu	0.507	0.578	0.552	0.569	0.597	0.642	0.593	0.608	0.599	0.607
Hf	3.08	3.42	3.44	3.65	3.80	3.93	3.69	3.85	3.83	3.85
Ta	0.156	0.261	0.176	0.184	0.190	0.609	0.188	0.192	0.194	0.190
Pb	6.59	7.12	6.62	6.87	7.55	7.65	7.46	7.66	7.73	7.80
Pb XRF	6.0		6.0	6.0	7.0		7.0	8.0	7.0	8.0
Th	1.657	1.662	1.743	1.890	1.986	1.892	1.912	1.993	2.028	2.033
U	0.869	0.925	0.974	1.024	1.055	1.074	1.029	1.056	1.085	1.078

Sample #	VULH-808B	VULK811	SER40	RP98020	RP96-030	RP96-049	RP96080	RP96100	RP97001
Date	19-Feb-98	19-Sep-94	30-Sep-94	1-Apr-95	21-Mar-96	11-May-96	4-Oct-96	4-Oct-96	9-Jan-97
SiO2	63.19	62.77	62.22	61.43	63.00	60.44	61.51	59.90	60.17
TiO2	0.910	0.907	0.910	0.880	0.910	0.890	0.907	0.880	0.873
Al2O3	15.75	15.88	15.80	15.72	15.74	15.65	15.43	15.58	15.53
Fe2O3	6.20	6.34	6.53	6.64	6.30	7.02	6.37	7.29	7.17
MnO	0.162	0.161	0.165	0.162	0.164	0.169	0.162	0.166	0.166
MgO	1.79	1.89	2.26	2.81	1.83	3.25	1.90	3.70	3.55
CaO	4.45	4.64	5.25	5.37	4.66	6.21	4.72	6.45	6.27
Na2O	4.60	4.61	4.44	4.20	4.65	4.07	4.72	3.99	4.11
K2O	2.62	2.54	2.48	2.32	2.60	2.24	2.54	2.11	2.16
P2O5	0.360	0.360	0.330	0.320	0.350	0.310	0.358	0.290	0.312
S	0.044	0.021	0.006	0.040	0.007	0.004	0.015	0.019	0.014
Total	100.08	100.11	100.39	99.89	100.21	100.25	98.62	100.39	100.33
ppm	SN-ICPMS	SN-ICPMS	LA-ICPMS		LA-ICPMS	LA-ICPMS	LA-ICPMS	LA-ICPMS	LA-ICPMS
Sc XRF	18.6	18.3	20.0	22.0	20.0	26.0	18.0	26.0	24.0
V XRF	91	100	106	114	98	138	89	139	127
Cr XRF	2	3	11	12	2	34	2	41	42
Ni XRF	<1	<1	4	2	<1	14	<1	19	19
Cu XRF	23	23	25	21	20	35	20	37	34
Zn XRF	96	97	86	86	90	90	85	94	85
Ga XRF	17.0	17.0	16.0	17.0	16.0	16.0	16.0	16.0	15.5
Rb	35.4	35.4	30.6		32.1	27.1	32.3	27.5	28.7
Rb XRF	35.0	34.0	31.0	32.7	33.0	29.0	32.0	26.5	27.0
Sr	359	360	349		347	349	356	370	375
Sr XRF	358	369	349	366	347	349	356	357	355
Y	39.9	38.6	36.5		38.0	32.9	38.1	33.8	35.7
Y XRF	35.0	35.0	31.0	34.5	33.0	29.0	33.0	28.0	29.0
Zr	150.1	146.6	139.8		144.2	122.0	144.4	124.2	131.5
Zr XRF	144.0	140.0	129.0	131.8	137.0	115.0	140.0	115.0	118.0
Nb	3.23	3.13	2.80		3.02	2.54	3.07	2.47	2.77
Nb XRF	2.0	2.0	2.0	3.1	2.0	2.0	3.0	2.0	2.0
Cs	0.963	0.945							
Ba	438	418	385		403	344	397	344	361
Ba XRF	415	400	380	376	410	355	390	345	345
La	14.00	13.91	13.35		14.00	11.97	13.78	11.83	12.52
Ce	31.91	31.67	29.52		30.87	26.08	30.36	26.08	27.82
Ce XRF	34	32	30	28	34	28	32	28	28
Pr	4.71	4.65	4.31		4.57	3.95	4.48	3.85	4.12
Nd	21.50	20.97	20.29		21.01	18.14	20.89	18.41	19.00
Sm	5.54	5.38	5.35		5.61	4.87	5.57	4.96	5.01
Eu	1.553	1.539	1.529		1.569	1.406	1.595	1.455	1.494
Gd	6.03	5.84	5.93		6.09	5.36	5.99	5.33	5.71
Tb	0.969	0.951							
Dy	6.01	5.85	6.07		6.28	5.48	6.22	5.50	5.83
Ho	1.320	1.298							
Er	3.91	3.82	3.92		3.98	3.53	3.94	3.58	3.73
Yb	3.86	3.80	3.94		4.05	3.61	4.00	3.47	3.86
Lu	0.597	0.589	0.637		0.653	0.564	0.638	0.578	0.594
Hf	3.78	3.67	3.91		4.03	3.37	3.91	3.49	3.73
Ta	0.191	0.188	0.191		0.194	0.168	0.250	0.205	0.213
Pb	7.94	7.64	7.18		7.91	7.01	7.02	8.69	7.62
Pb XRF	8.0	7.0	7.0	8.5	7.0	6.0	6.0	7.0	6.0
Th	2.009	1.942	1.844		1.942	1.617	1.919	1.676	1.745
U	1.072	1.062	1.049		1.063	0.917	1.086	0.919	0.992

Sample #	RP97030	RP97212	RP97222	RP97215M3	RP98048	RP98051	rp99007	rp99011	RP0015p17
Date	7-Feb-97	5-Apr-97	10-Apr-97	13-Apr-97	20-Aug-98	20-Aug-98	21-Apr-99	*15-Jul-99*	11-Nov-00
SiO2	63.17	58.03	63.14	58.29	61.47	62.19	62.46	59.90	62.85
TiO2	0.910	0.825	0.914	0.857	0.906	0.907	0.921	0.877	0.928
Al2O3	15.80	15.84	15.80	15.74	15.86	15.76	15.74	15.72	15.79
Fe2O3	6.43	7.49	6.41	7.71	6.79	6.48	6.47	6.82	6.56
MnO	0.166	0.167	0.165	0.171	0.165	0.163	0.164	0.158	0.168
MgO	1.92	4.48	1.90	4.34	2.61	2.13	1.99	2.50	1.95
CaO	4.72	7.59	4.73	7.53	5.48	4.94	4.83	5.80	4.76
Na2O	4.56	3.63	4.59	3.62	4.35	4.52	4.54	4.14	4.64
K2O	2.54	1.85	2.53	1.90	2.35	2.47	2.54	2.19	2.54
P2O5	0.357	0.274	0.358	0.269	0.334	0.347	0.357	0.321	0.356
S	0.024	0.013	0.015	0.005	0.010	0.015	0.009	0.498	0.006
Total	100.59	100.17	100.56	100.43	100.33	99.91	100.01	98.92	100.54
ppm	LA-ICPMS		LA-ICPMS	LA-ICPMS			LA-ICPMS		LA-ICPMS
Sc XRF	19.0	27.0	19.0		22	20	20	26	19.3
V XRF	93	144	93	193	112	100	96	132	133
Cr XRF	4	65	4	54	18	8	4	16	6
Ni XRF	<1	29	<1	23	8	2	<2	8	
Cu XRF	22	40	21	54	28	24	24	40	
Zn XRF	88	82	87	90	81	82	84	96	
Ga XRF	16.5	15.5	16.0	16.8	17.1	16.9	16.6	16.5	17.4
Rb	33.6	27.9	33.6	25.4			31.9		32.4
Rb XRF	32.5	23.0	32.5	27.7	33.0	34.9	36.2	32.0	32.4
Sr	360	395	362	397			357		326
Sr XRF	352	363	352	397	372	366	355	364	
Y	39.4	30.7	39.4	32.0			37.8		37.1
Y XRF	33.0	26.0	33.0	30.6	35.4	36.1	37.5	34.1	
Zr	152.4	105.4	151.4	111.5			145.4		145.7
Zr XRF	140.0	103.0	140.0	104.0	129.7	136.6	139.2	120.7	
Nb	3.17	2.65	3.23	2.30			3.01		3.05
Nb XRF	3.0	2.0	3.0	2.8	2.6	2.4	2.6	1.9	
Cs							0.795		0.824
Ba	409	309	411	319			387		390
Ba XRF	410	300	405	309	360	364	405	340	
La	14.41		14.33	10.95			13.62		13.68
Ce	31.72		31.72	24.30			30.00		30.18
Ce XRF	32	26	36	19	26	27	35	30	
Pr	4.70		4.63	3.59			4.37		4.44
Nd	21.82		21.79	16.67			18.51		18.77
Sm	5.76		5.80	4.64			5.38		5.46
Eu	1.674		1.656	1.357			1.495		1.473
Gd	6.29		6.29	5.04			5.93		5.92
Tb									
Dy	6.37		6.52	5.19			6.38		6.45
Ho									
Er	4.19		4.23	3.41			3.85		3.88
Yb	4.21		4.18	3.36			3.94		4.05
Lu	0.668		0.682	0.523			0.645		0.663
Hf	4.25	4.05	4.23	3.07			4.40		4.26
Ta	0.225		0.246	0.204			0.235		0.217
Pb	8.09		7.60	6.48			9.51		10.48
Pb XRF	7.0	5.0	8.0	7.5	7.0	7.5	9.0	10.0	
Th	2.060		2.025	1.503			1.868		2.024
U	1.141		1.127	0.823			1.036		1.149

Table 3. Least squares mixing model results

Phenocrysts	SiO2	TiO2	Al2O3	Fe2O3	MnO	MgO	CaO	Na2O	K2O	P2O5	Cr2O3
Ol Fo84	39.74	0.00	0.00	15.21	0.251	44.56	0.244	0.00	0.00	0.00	0.000
Cpx Mg84	50.81	0.417	4.40	4.76	0.000	15.45	23.54	0.327	0.00	0.00	0.296
Plag An93.5	44.11	0.00	34.75	0.611	0.059	0.148	19.56	0.765	0.00	0.00	0.000
Opx Mg#75	53.64	0.230	0.666	17.55	0.709	25.38	1.568	0.262	0.00	0.00	0.000
Cpx Mg#75	51.30	0.548	2.051	9.27	0.264	15.35	20.72	0.509	0.00	0.00	0.000
Plag An60	52.92	0.00	28.93	0.732	0.00	0.114	12.55	4.53	0.235	0.00	0.000
Ol Fo70	37.82	0.00	0.00	26.55	0.574	34.86	0.192	0.00	0.00	0.00	0.000
Plag An70	50.47	0.00	30.90	0.797	0.00	0.117	14.23	3.39	0.095	0.00	0.000
Magnetite	0.00	12.31	3.13	80.34	0.587	3.434	0.00	0.00	0.00	0.00	0.199
Apatite	56.00	0.00	0.00	0.00	0.00	0.00	0.00	0.00	0.00	44.00	0.000
Whole-rock compositions	SiO2	TiO2	Al2O3	Fe2O3	MnO	MgO	CaO	Na2O	K2O	P2O5	Cr2O3
Vulcan'94*	62.92	0.904	15.73	6.28	0.159	1.860	4.59	4.61	2.56	0.356	0.00
Vulcan'37*	63.59	0.895	15.55	5.88	0.159	1.627	4.32	4.61	2.72	0.360	0.00
Vulcan'78*	62.72	0.904	15.70	6.10	0.155	1.709	4.70	4.44	2.61	0.371	0.00
Tav817	60.05	0.890	16.04	7.09	0.160	2.84	6.19	4.10	2.12	0.290	0.00
Tav98-012	57.76	0.850	15.68	7.88	0.170	4.46	7.39	3.67	1.86	0.270	0.01
Tavurvur Phase2*	62.44	0.915	15.78	6.45	0.164	1.987	4.82	4.57	2.51	0.355	0.00
Vul'37 2014	49.88	0.800	15.31	10.45	0.180	7.93	12.42	2.18	0.63	0.160	0.03
Palangiangia#5	48.44	0.800	18.12	10.85	0.180	6.31	12.89	1.82	0.46	0.120	0.01
PraedPoint#13d	48.38	0.810	19.19	10.51	0.180	5.41	12.82	2.17	0.42	0.110	0.00
1400BP*	65.88	0.838	15.22	5.13	0.155	1.347	3.44	4.85	2.97	0.275	0.00

Results

Whole-rock		Vulcan 1937			Plag An60	Cpx Mg#75	Opx Mg#75	Magnetite	Apatite	TOTAL	RSSQ
Vulcan 1878*	=	95.35			2.87	1.09	-0.07	0.48	0.08	99.8	0.009
		Vulcan 1937			Plag An70	Cpx Mg#75	Opx Mg#75	Magnetite	Apatite		
Vulcan 1878*	=	95.82			2.48	1.02	-0.06	0.45	0.07	99.8	0.005
Vulcan 1994*	=	95.91			2.56	0.31	0.88	0.54	0.01	100.2	0.012
		#Vul822	Vul'37 2014	Ol Fo84							
#Tav98-012	=	62.7	36.4	0.93						99.9	0.032
#Tav817	=	79.9	20.5	-0.59						99.8	0.060
		#Vul822		Ol Fo84		Plag An93.5	Cpx Mg#84	Magnetite			
Palangiangia #5	=	34.1		5.1		33.2	20.4	8.4		101.1	0.572
Praed Point #13d	=	35.1		4.0		36.2	17.3	8.2		100.9	0.635
		1400BP*			Plag An60	Cpx Mg#75	Opx Mg#75	Magnetite	Apatite		
Vulcan'94*	=	85.19			9.19	2.34	1.10	1.77	0.27	99.9	0.005
		Vul'37 2014	Vulcan 1994*								
Tavurvur Phase2*	=	3.1	96.8							99.9	0.014

Mixing calculations performed using MINSQ (Herrmann and Berry, 2002)

* average dacite compositions calculated for Vulcan 1878, 1937 and 1994 eruptions, and Tavurvur 1994-2001 Phase 2 eruption subsequent to July 1998.

HIGHLIGHTS - PATIA ET AL.

1. Whole-rock geochemical data and phenocryst mineral chemistry indicate the eruption of identical dacitic magmas in 1994 from the vents Vulcan and Tavurvur, on opposite sides of Rabaul Caldera, and provide evidence for a caldera-extensive dacitic magma reservoir.
2. Vulcan eruptives define a tight cluster of dacite compositions, whereas Tavurvur eruptives span an array from equivalent dacite compositions to mafic andesites.
3. The Tavurvur andesites form a linear compositional array and have strongly bimodal phenocryst assemblages that reflect dacite hybridisation with a mafic basalt.
4. The moderately large volume SO_2 flux documented in the Tavurvur volcanic plume (and negligible SO_2 flux in the Vulcan plume) combined with high dissolved S contents of basaltic melt inclusions trapped in olivine of Tavurvur eruptives, indicate that the amount of degassed basaltic magma was ~0.1 km^3 and suggest that the injection of this magma was confined to the Tavurvur-side (eastern to northeastern sector) of the caldera.
5. Circumstantial evidence suggests that the eruption was triggered and evolved in response to a series of basaltic magma injections that may have commenced in 1971 and continued up until at least the start of the 1994 eurptons.
6. The presence of zoned plagioclase phenocrysts reflecting older basalt-dacite interaction events, evaluation of limited available data for the products of previous eruptions in 1878 and 1937-1943, and the episodic occurrence of major intra-caldera seismo-deformational events indicate that the shallow magma system at Rabaul Caldera is subjected to repeated mafic magma injections at intervals of several years to several decades.